Table 3 Results of liver biopsy

	Simple steatosis	NASH
Stage: 1/2/3/4		13/13/13/2
Grade: 1/2/3		27/10/4
Iron: 0/1/2/3	11/12/3/1	14/8/6/6
Steatosis:		
<30%	14	18
30%–60%	7	13
60% <	2	10

NASH, nonalcoholic steatohepatitis.

patients than in the simple steatosis patients. Neither significant fibrosis nor inflammation was observed in the biopsy specimens from patients with simple steatosis. Six specimens from simple steatosis patients and seven specimens from NASH patients were not available for iron staining.

Hepatic oxidative stress

We evaluated hepatic oxidative stress by the level of hepatic Trx, since Trx is known to be a redox-sensitive molecule.[14] We have previously reported that serum Trx levels are a marker of NASH.[15] We measured hepatic thioredoxin mRNA, because it would reflect the redox status of the liver more precisely than serum thioredoxin levels. Hepatic thioredoxin consists of both reduced and oxidized forms, whereas serum thioredoxin is an oxidized form. Therefore, hepatic thioredoxin levels do not correlate with serum thioredoxin levels. The Trx level increased in the order of controls, then simple steatosis patients with the highest levels in NASH patients (Table 4). The differences among the groups were significant (Table 4). The Trx level tended to increase as the stage progressed; however, it did not show any association with the grade (Table 5).

Fatty acid metabolism

The levels of transcripts for the genes involved in fatty acid metabolism were increased in the order of controls, then NASH patients with the highest levels in simple steatosis patients (Table 4). The differences among the groups were significant (Table 4). When values were compared between simple steatosis and NASH patients by the Mann–Whitney's test, the difference was significant in FATP5 ($P < 0.01$), ACAC ($P < 0.05$), PPARα ($P < 0.05$), CYP2E1 ($P < 0.05$), ACADM ($P < 0.05$), ACOX ($P < 0.05$), MTP ($P < 0.05$). Levels of all these genes were significantly higher in the simple steatosis patients than the NASH patients. When compared with the liver histology, the levels of FATP5, SREBP1c, ACAC, PPARα, CYP2E1, ACADM and MTP significantly decreased as the stage and grade progressed (Table 5). The level of ACOX tended to decrease as the stage and grade progressed (Table 5). The level of FASN was similarly decreased, although the difference between groups

Table 4 The levels of hepatic gene involved in lipid and iron metabolism

	Control	Simple steatosis	NASH	*P* value
Trx	1.0 ± 1.1	2.3 ± 0.9	2.5 ± 1.0	$P < 0.00001$
FATP5	1.0 ± 0.4	6.1 ± 3.6	4.3 ± 2.5	$P < 0.00001$
SREBP1c	1.0 ± 0.6	73.9 ± 74.3	56.0 ± 85.4	$P < 0.00001$
FASN	1.0 ± 1.0	28.2 ± 26.8	17.8 ± 15.1	$P < 0.00001$
ACAC	1.0 ± 0.8	12.2 ± 5.9	8.7 ± 3.4	$P < 0.00001$
PPARα	1.0 ± 0.8	21.1 ± 11.3	15.5 ± 8.1	$P < 0.00001$
CYP2E1	1.0 ± 0.4	8.0 ± 4.2	6.2 ± 3.2	$P < 0.00001$
ACADM	1.0 ± 0.9	17.8 ± 9.7	13.1 ± 6.1	$P < 0.00001$
ACOX	1.0 ± 0.9	16.6 ± 9.2	12.0 ± 5.7	$P < 0.00001$
MTP	1.0 ± 1.0	10.8 ± 3.8	8.8 ± 3.3	$P < 0.00001$
TfR1	1.0 ± 1.1	10.8 ± 11.3	11.8 ± 10.3	$P < 0.00001$
TfR2	1.0 ± 0.4	7.6 ± 3.6	5.6 ± 2.8	$P < 0.00001$
hepcidin	1.0 ± 0.9	11.2 ± 9.6	5.7 ± 3.9	$P < 0.00001$

Note: The value is expressed as folds to mean control values (mean ± S.D.). The deference between the groups was determined using the Kruskal–Wallis test.
Trx, thioredoxin; FATP5, fatty acid transport protein 5; SREBP1c, sterol regulatory element-binding protein 1c; FASN, fatty acid synthase; ACAC, acetyl-coenzyme A carboxylase; PPARα, peroxisome proliferative activated receptor α; CYP2E1, cytochrome P-450 2E1; ACADM, acyl-coenzyme A dehydrogenase; ACOX, acyl-coenzyme A oxidase; MTP, microsomal triglyceride transfer protein; TfR1, transferrin receptor 1, TfR2, transferrin receptor 2.

Table 5 Correlation of the gene levels with liver histology*

	Stage		Grade	
	r	*P* value	*r*	*P* value
Trx	0.209	0.074	0.132	0.266
FATP5	−0.334	0.004	−0.339	0.003
SREBP1c	−0.264	0.024	−0.283	0.015
FASN	−0.158	0.178	−0.182	0.124
ACAC	−0.264	0.024	−0.313	0.007
PPARα	−0.253	0.031	−0.244	0.038
CYP2E1	−0.264	0.024	−0.293	0.012
ACADM	−0.241	0.040	−0.246	0.036
ACOX	−0.213	0.070	−0.213	0.071
MTP	−0.262	0.025	−0.271	0.020
TfR1	0.227	0.037	0.182	0.089
TfR2	−0.307	0.008	−0.318	0.006
hepcidin	−0.251	0.032	−0.221	0.060

*Using Spearman's test. Trx, thioredoxin; FATP5, fatty acid transport protein 5, SREBP1c, sterol regulatory element-binding protein 1c; FASN, fatty acid synthase; ACAC, acetyl-coenzyme A carboxylase; PPARα, peroxisome proliferative activated receptor α; CYP2E1, cytochrome P-450 2E1, ACADM, acyl-coenzyme A dehydrogenase; ACOX, acyl-coenzyme A oxidase; MTP, microsomal triglyceride transfer protein; TfR1, transferrin receptor 1, TfR2, transferrin receptor 2.

did not reach statistical significance (Table 5). In parallel with these findings, the level of hepatic steatosis decreased as the stage and grade progressed (Fig. 1). None of these genes was independently correlated with hepatic steatosis (not shown).

TfR1 and TfR2

The hepatic iron score (HIS) tended to increase as the stage progressed (Table 6). We examined the levels of TfR1 and TfR2, since the uptake of serum iron by hepatocytes is largely through a transferrin-bound form.[16] The levels of both of these genes were significantly higher in the NAFLD patients than in the controls (Table 4). When values were compared between simple steatosis and NASH using the Mann–Whitney's test, the TfR2 level was significantly ($P < 0.01$) higher in the simple steatosis patients than the NASH patients. The TfR1 level significantly increased as the stage progressed, whereas that of TfR2 significantly decreased as the stage and grade progressed (Table 5). Neither TfR1 nor TfR2 were independently correlated with HIS (not shown).

Table 6 Hepatic iron score and the stage

	Hepatic iron score				
	0	1	2	3	4
Stage 0	11	11	3	0	1
Stage 1	7	1	1	1	0
Stage 2	3	4	3	2	0
Stage 3	4	4	2	2	0
Stage 4	0	0	0	0	1

Note: The value represents the number of patients. Simple steatosis was considered as stage "0" $r = 0.213$, $P = 0.099$, iron score *vs* stage: Spearman's test.

Hepcidin

Hepcidin is known to be secreted from hepatocytes and regulates systemic iron transport.[16] The hepcidin level was significantly different among the controls, the simple steatosis patients and the NASH patients. The value was higher in the simple steatosis patients than in the NASH patients (Table 4). Hepcidin level decreased significantly as the stage progressed (Table 5). Since the ratio of hepcidin to iron load has been reported to evaluate the appropriateness of the hepcidin response to iron overload,[17] we divided hepcidin mRNA levels by serum ferritin levels or HIS. The ratios of hepcidin mRNA/ferritin and hepcidin mNA/HIS were signifi-

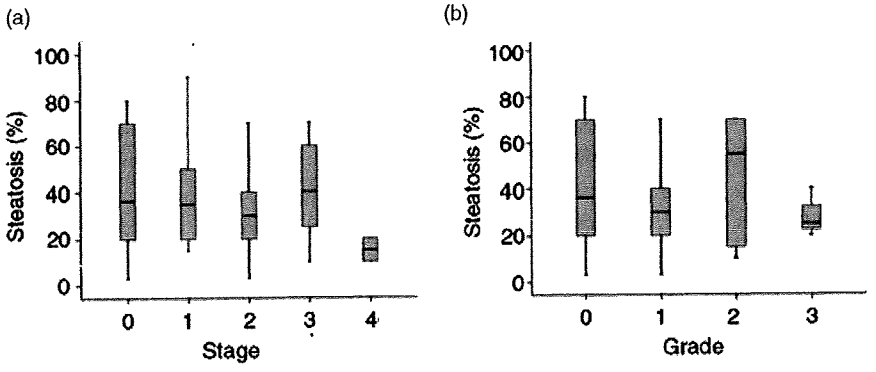

Figure 1 Distributions of the level of hepatic steatosis in association with the stage (a) and grade (b). The level of steatosis decreased as the stage and grade progressed.

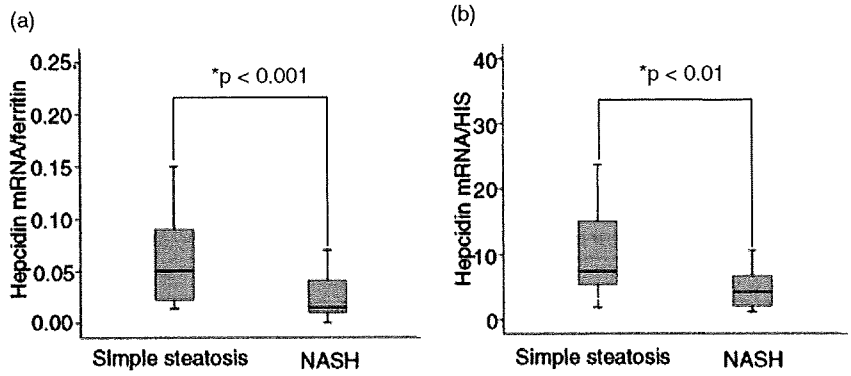

Figure 2 The ratio of hepcidin mRNA levels to serum ferritin levels (a) and that of hepcidin mRNA levels to hepatic iron score (HIS) (b). Hepcidin mRNA levels corrected for iron overload were significantly lower in NASH patients than in simple steatosis patients. *Mann-Whitney U-test.

cantly lower in NASH patients than simple steatosis patients (Fig. 2). The ratio of hepcidin mRNA/ferritin was significantly correlated with stage ($r = -0.523$, $P < 0.00005$) and grade ($r = -0.436$, $P < 0.0005$). The same results were obtained from the ratio of hepcidin mRNA/HIS ($r = -0.424$, $P < 0.01$ vs stage; $r = -0.373$, $P < 0.05$ vs grade). We compared hepcidin mRNA levels with metabolic variables and found that the level of hepcidin was significantly correlated with both total cholesterol ($r = 0.323$, $P < 0.01$) and triglyceride ($r = 0.323$, $P < 0.01$). The ratio of hepcidin mRNA/ferritin was also significantly correlated with total cholesterol ($r = 0.365$, $P < 0.005$).

DISCUSSION

IN THIS STUDY, we investigated the expression levels of hepatic genes that play significant roles in the metabolism of fatty acids and iron. Their roles in hepatocytes include the uptake, synthesis, oxidation, storage and excretion of fatty acids,[10,18,19] the uptake of iron and the regulation of systemic iron transport.[16] We found that the levels of these genes were significantly higher in NAFLD patients than controls. In addition, we found some novel findings. However, none of the individual genes was independently correlated with hepatic steatosis. These results indicated that neither the lack of nor increase in the expression levels of any of these genes plays an independent role in the development of fatty liver.

Insulin resistance is the "first hit" in the development of NASH,[9] which is characterized by an increase in the uptake and synthesis of fatty acids in hepatocytes.[19] Nevertheless, our results showed that the levels of fatty acid-related genes decreased in the later stages despite the presence of insulin resistance. In parallel with these findings, the level of hepatic steatosis also decreased. Considering that fat is the fuel involved in progressive liver injuries,[20] these findings might be associated with "burn-out" NASH.[21] Although the underlying reason for this is unclear, some possibilities should be considered. Because hepatic adenosine 5′-triphosphate (ATP) levels tend to be decreased in fatty liver,[22] hepatic adenosine monophosphate-activated protein kinase (AMPK) should be activated.[23] AMPK is known to activate catabolic pathways and switch off protein, carbohydrate and lipid synthesis, such that cellular energy levels remain unchanged.[23] Thus, activated AMPK in hepatocytes might contribute to the decrease in the expression levels of fatty acid-related genes. Anti-diabetic drugs, which ameliorate liver injuries in patients with NASH, have been reported to activate AMPK.[24] Interestingly, the levels of all the genes involved in fatty acid metabolism were lower in the patients treated with insulin sensitizers than in those treated with other agents or followed with diet restriction. Statistical significance was achieved only in FATP5 ($P < 0.05$, Mann–Whitney's test). However, these results may be difficult to evaluate or apply generally, because the numbers of patients were small.

Hepatic iron load has been documented to be another key player in the progression from steatosis to steatohepatitis.[11] Hepatic iron load has been attributed to the Cys282Tyr mutation in the hemochromatosis gene.[11] This mutation decreases hepatic synthesis of hepcidin, resulting in the facilitation of iron absorption from the duodenum.[16] Our results showed that hepatic iron scores tended to correlate with the histological stage of NAFLD. Furthermore, the ratios of hepcidin mRNA/ferritin and hepcidin mRNA/HIS were significantly lower in NASH patients than in simple steatosis patients. This insufficient production of hepcidin may not be attributed to the genetic mutation, since known mutations of hemochromatosis-associated genes have been reported to be rare among Japanese patients.[25]

Interestingly, the hepcidin level was significantly correlated with the levels of total cholesterol and triglycerides. These findings coincide with those recently reported by Barisani *et al.*,[17] who reported that the hepcidin mRNA/ferritin ratio and the hepcidin mRNA/tissue iron score ratio were significantly lower in the NAFLD group with hepatic iron overload than in the NAFLD group without iron overload,[17] and that the level of hepatic hepcidin mRNA was significantly correlated with lipid parameters.[17] Our findings, in concert with those of Barisani *et al.*, suggest that more severe forms of NAFLD are associated with insufficient hepcidin production, and that lipid metabolism might be involved in hepcidin synthesis. Alternatively, the hepatic levels of TfR1 and TfR2 were significantly higher in NAFLD patients than controls. Therefore, TfR1 and TfR2 would be expected to promote hepatic iron load irrespective of iron absorption from the duodenum.

TfR1 is ubiquitously expressed in the human body,[16] while TfR2 is dominantly expressed in specific organs including the liver.[26] TfR1 has a high affinity with transferrin[27] and its expression is regulated by the iron-responsive element (IRE) in the 3′-untranslated regions of mRNAs.[16] In the NAFLD patients, the TfR1 level increased significantly as the stage progressed. Since ROS stabilize TfR1 mRNA via activation of iron regulatory proteins that interact with IRE,[16] hepatic oxidative stress should upregulate TfR1 in NAFLD.

TfR2 was recently identified as a novel transferrin receptor,[26] although the expression mechanisms have not been fully determined.[28] Similarly, neither the physiological nor pathological role of TfR2 in the liver has been documented. The expression level of TfR2 was higher in NAFLD patients than controls. At present, the association between the level of TfR2 and the pathogenesis of NAFLD remains unknown. Regardless of the role of TfR2, we have reported that the TfR2 level is significantly correlated with that of PPARα.[29] It is of much interest to speculate that PPARα might contribute to the regulation of TfR2, since PPARα may be upregulated in NAFLD by intrinsic PPARα ligands. This hypothesis is under investigation in our institute.

In summary, we investigated the metabolism of fatty acids and iron in the livers of NAFLD patients. Steatosis-related metabolism is attenuated as the disease progresses, whereas iron load-related metabolism is exacerbated. Based on these findings, we hypothesize that anti-lipid synthesis should be considered in the early stages and that iron reduction should be considered in the later stages. The former therapies may thus include body weight reduction and insulin-sensitizing drugs, and the latter therapies may include phlebotomy, iron-restriction diets and/or antioxidants.

REFERENCES

1 Angulo P. Nonalcoholic fatty liver disease. *N Engl J Med* 2002; 346: 1221–31.
2 Hui JM, Kench JG, Chitturi S *et al.* Long-term outcomes of cirrhosis in nonalcoholic steatohepatitis compared eith hepatitis C. *Hepatology* 2003; 38: 420–7
3 Ratziu V, Bonyhay L, Di Martino V *et al.* Survival, liver failure, and hepatocellular carcinoma in obesity-related cryptogenic cirrhosis. *Hepatology* 2002; 35: 1485–93.
4 Suzuki A, Lindor K, St Saver J *et al.* Effect of changes on body weight and lifestyle in nonalcoholic fatty liver disease. *J Hepatol* 2005; 43: 1060–6.
5 Marchesini G, Brizi M, Bianchi G, Tomassetti S, Zoli M, Melchionda N. Metformin in non-alcoholic steatohepatitis. *Lancet* 2001; 358: 893–4.
6 Abdelmalek MF, Angulo P, Jorgensen RA, Sylvestre PB, Lindor KD. Betaine, a promising new agent for patients with nonalcoholic steatohepatitis: results of a pilot study. *Am J Gastroenterol* 2001; 96: 2711–7.
7 Facchini FS, Hua NW, Stoohs RA. Effect of iron depletion in carbohydrate-intolerant patients with clinical evidence of nonalcoholic fatty liver disease. *Gastroenterology* 2002; 122: 931–9
8 Lindor KD, Kowdley KV, Heathcote EJ *et al.* Ursodeoxycholic acid for treatment of nonalcoholic steatohepatitis: results of a randomized trial. *Hepatology* 2004; 39: 770–8.
9 Day CP, James OF. Steatohepatitis: a tale of two "hits"? *Gastroenterology* 1998; 114: 842–5.
10 Browning JD, Horton JD. Molecular mediators of hepatic steatosis and liver injury. *J Clin Invest* 2004; 114: 147–52.
11 George DK, Goldwurm S, MacDonald GA *et al.* Increased hepatic iron concentration in nonalcoholic steatohepatitis is associated with increased fibrosis. *Gastroenterology* 1998; 114: 311–8.
12 Brunt EM, Janney CG, Di Bisceglie AM, Neuschwander-Tetri BA, Bacon BR. Nonalcoholic steatohepatitis: a proposal for grading and staging the histological lesions. *Am J Gastroenterol* 1999; 94: 2467–74.
13 Searle J, Kerr JFR, Halliday JW, Powell LW. Iron storage disease. In: MacSween RNM, Anthony PP, Scheuer PJ, eds. *Pathology of the Liver*, 3rd edn. London: Churchill Livingstone, 1994; 219–41.
14 Hirota K, Nakamura H, Masutani H, Yodoi J. Thioredoxin superfamily and thioredoxin-inducing agents. *Ann N Y Acad Sci* 2002; 957: 189–99.
15 Sumida Y, Nakashima T, Yoh T *et al.* Serum thioredoxin levels as a predictor of steatohepatitis in patients with nonalcoholic fatty liver disease. *J Hepatol* 2003; 38: 32–8.
16 Hentze MW, Muckenthaler MU, Andrews NC. Balancing acts: molecular control of mammalian iron metabolism. *Cell* 2004; 117: 285–97

17 Barisani D, Pelucchi S, Mariani R *et al.* Hepcidin and iron-related gene expression in subjects with Dysmetabolic Hepatic Iron Overload. *J Hepatol* 2008; **49**: 123–33.
18 Doege H, Baillie RA, Ortegon AM *et al.* Targeted deletion of FATP5 reveals multiple functions in liver metabolism: alterations in hepatic lipid homeostasis. *Gastroenterology* 2006; **130**: 1245–58.
19 Goldberg IJ, Ginsberg HN. Ins and outs modulating hepatic triglyceride and development of nonalcoholic fatty liver disease. *Gastroenterology* 2006; **130**: 1343–6.
20 Day CP, James OF Hepatic steatosis: innocent bystander or guilty party? *Hepatology* 1998; **27**: 1463–6.
21 Caldwell SH, Oelsner DH, Iezzoni JC, Hespenheide EE, Battle EH, Driscoll CJ. Cryptogenic cirrhosis: clinical characterization and risk factors for underlying disease. *Hepatology* 1999; **29**: 664–9.
22 Chavin KD, Yang S, Lin HZ *et al.* Obesity induces expression of uncoupling protein-2 in hepatocytes and promotes liver ATP depletion. *J Biol Chem* 1999; **274**: 5692–700.
23 Hardie DG, Scott JW, Pan DA, Hudson ER. Management of cellular energy by the AMP-activated protein kinase system. *FEBS Lett* 2003; **546**: 113–20.
24 Fryer LG, Parbu-Patel A, Carling D. The anti-diabetic drugs rosiglitazone and metformin stimulate AMPK-activated protein kinase through distinct signaling pathways. *J Biol Chem* 2002; **277**: 25226–32.
25 Yamauchi N, Itoh Y, Tanaka Y *et al.* Clinical characteristics and prevalence of GB virus C, SEN virus, and HFE gene mutation in Japanese patients with nonalcoholic steatohepatitis. *J Gastroenterol* 2004; **39**: 654–60.
26 Kawabata H, Yang R, Hirama T *et al.* Molecular cloning of transferring receptor 2. *J Biol Chem* 1999; **274**: 20826–32.
27 Robb AD, Ericsson M, Wessling-Resnick M. Transferrin receptor 2 mediates a biphasic pattern of transferrin uptake associated with ligand delivery to multivesicular bodies. *Am J Physiol Cell Physiol* 2004; **287**: 1769–75.
28 Kawabata H, Germain RS, Ikezoe T *et al.* Regulation of expression of murine transferrin receptor 2. *Blood* 2001; **98**: 1949–54.
29 Mitsuyoshi H, Yasui K, Harano Y, Itoh Y, Okanoue T. Analysis of hepatic expression of genes involved in lipid and iron metabolism in nonalcoholic fatty liver disease. *Hepatology* 2007; **46**: 733A.

Cancer Letters 275 (2009) 27–34

Contents lists available at ScienceDirect

Cancer Letters

journal homepage: www.elsevier.com/locate/canlet

A novel amplification target, *ARHGAP5*, promotes cell spreading and migration by negatively regulating RhoA in Huh-7 hepatocellular carcinoma cells

Yasuyuki Gen [a], Kohichiroh Yasui [a,*], Keika Zen [a], Tomoaki Nakajima [a], Kazuhiro Tsuji [a], Mio Endo [a], Hironori Mitsuyoshi [a], Masahito Minami [a], Yoshito Itoh [a], Shinji Tanaka [b], Masafumi Taniwaki [c], Shigeki Arii [b], Takeshi Okanoue [a,d], Toshikazu Yoshikawa [a]

[a] *Molecular Gastroenterology and Hepatology, Graduate School of Medical Science, Kyoto Prefectural University of Medicine, 465 Kajii-cho, Kamigyo-ku, Kyoto 602-8566, Japan*
[b] *Department of Hepato-Biliary-Pancreatic Surgery, Tokyo Medical and Dental University, Tokyo, 1-5-45 Yushima, Bunkyo-ku, Tokyo 113-8510, Japan*
[c] *Molecular Hematology and Oncology, Graduate School of Medical Science, Kyoto Prefectural University of Medicine, Kyoto, 465 Kajii-cho, Kamigyo-ku, Kyoto 602-8566, Japan*
[d] *Department of Hepatology, Saiseikai Suita Hospital, Suita, Osaka 564-0013, Japan*

ARTICLE INFO

Article history:
Received 19 August 2008
Received in revised form 23 September 2008
Accepted 30 September 2008

Keywords:
ARHGAP5
p190-B RhoGAP
RhoA
Amplification
Hepatocellular carcinoma

ABSTRACT

RhoA, a member of the Rho family of small GTPases, directs the organization of the actin cytoskeleton and is involved in regulating cell shape and movement. Its activity is negatively regulated by p190-B RhoGAP (GTPase-activating protein). We investigated DNA copy number aberrations in human hepatocellular carcinoma and esophageal squamous cell carcinoma cell lines using a high-density oligonucleotide microarray and found a novel amplification at chromosomal region 14q12. We identified *ARHGAP5* (the gene encoding p190-B RhoGAP) as a probable target for the amplification at 14q12, and our results showed that p190-B RhoGAP promotes cells spreading and migration by negatively regulating RhoA activity in Huh-7 hepatocellular carcinoma cells.

1. Introduction

Members of the Rho family of small GTPases act as molecular switches. In response to extracellular signals, they direct the organization of the actin cytoskeleton and alter gene expression [1]. Rho proteins, which include the much-studied Cdc42, Rac1 and RhoA, are involved in regulating cell shape, polarity and movement and establishing cell-cell junctional complexes. Accordingly, their activity is tightly controlled by regulatory proteins that determine whether GTP or GDP is bound. Rho proteins are activated by guanine nucleotide exchange factors, which catalyze the release of GDP and thus allow GTP to bind the proteins. Rho proteins in turn are inactivated by Rho GTPase-activating proteins (GAPs), which bind to the Rho proteins and induce them to hydrolyze their bound GTP to GDP. p190-B RhoGAP, a member of the RhoGAP family, negatively regulates RhoA activity [2,3].

Amplification of DNA in certain regions of chromosomes plays a crucial role in the development and progression of human malignancies, specifically when proto-oncogenic target genes within those amplicons are overexpressed. Oncogenes that are often amplified in cancers include *MYC*, *ERBB2* and *CCND1*.

In the present study, we investigated DNA copy number aberrations in human hepatocellular carcinoma (HCC) and

* Corresponding author. Tel.: +81 75 251 5519; fax: +81 75 251 0710.
E-mail address: yasuik@koto.kpu-m.ac.jp (K. Yasui).

0304-3835/$ - see front matter © 2008 Elsevier Ireland Ltd. All rights reserved.
doi:10.1016/j.canlet.2008.09.036

esophageal squamous cell carcinoma (ESCC) cell lines and found a novel amplification at chromosomal region 14q12. Because the region may harbor one or more proto-oncogenes whose overexpression following amplification contributes to the initiation or progression of HCC and ESCC, we carried out molecular definition of the amplicon. We show here that the p190-B RhoGAP gene (*ARHGAP5*) within the 14q12 amplicon is amplified and overexpressed, and that p190-B RhoGAP promotes cell spreading and migration in Huh-7 hepatocellular carcinoma cells.

2. Materials and methods

2.1. Cell lines

A total of 10 HCC cell lines (JHH-6, JHH-7, SNU354, SNU398, SNU423, SNU475, Huh-1, Huh-7, HLE and PLC/PRF/5) and 10 ESCC cell lines (T.T, EC-GI-10, KYSE140, KYSE220, TE-4, TE-5, TE-6, TE-10, TE-14 and TE-15) were examined. All cell lines were maintained in Dulbecco's modified Eagle's medium (DMEM) supplemented with 10% fetal calf serum (FCS). Genomic DNA was isolated from each cell line using the Puregene DNA isolation kit (Gentra, Minneapolis, MN, USA).

2.2. Array analysis

Array analyses were performed using the GeneChip Mapping 250K Sty array (Affymetrix, Santa Clara, CA, USA) according to the manufacturer's instructions. In brief, 250 ng of genomic DNA was digested with a restriction enzyme (StyI), ligated to an adaptor and amplified by PCR. Amplified products were fragmented, labeled by biotinylation and hybridized to the microarrays. Hybridization was detected by incubation with streptavidin–phycoerythrin conjugate, and the array was scanned. Analysis was performed as previously described [4]. Copy number changes were calculated using the Copy Number Analyzer for Affymetrix GeneChip Mapping Arrays (CNAG; http://www.genome.umin.jp) [5].

2.3. Fluorescence in situ hybridization (FISH)

We performed FISH using three bacterial artificial chromosomes (BACs), RP11-113E19, RP11-431H16 and RP11-54H22 as probes (Invitrogen, Carlsbad, CA, USA), as described previously [6]. The BACs were selected based on homology with locations in the human genome according to the database provided by the UCSC (http://genome.ucsc.edu/).

2.4. Real-time quantitative PCR

We quantified genomic DNA and mRNA using a real-time fluorescence detection method, as described previously [6]. The primers used were as follows: *ARHGAP5* mRNA (forward, 5′-CATCTGTTTTTGGCCAACCT-3′; reverse, 5′-gtggaggagccacaatgttt-3′); *HEATR5A* mRNA (forward, 5′-TGTGCCTCCTACTCATGCTG-3′; reverse, 5′-gagatggcctgagct tgaac-3′); *c14orf126* mRNA (forward, 5′-gtgctttttcaaggga gctg-3′; reverse, 5′-ttcctccaagggtagcttga-3′); *NUBPL* mRNA (forward, 5′-cttggccttgtccaaaacat-3′; reverse, 5′-acaattggc tggcctgtatc-3′). These primers were designed using Primer3 (http://frodo.wi.mit.edu/cgi-bin/primer3/primer3_www.cgi) based on sequence data obtained from the NCBI database (http://www.ncbi.nlm.nih.gov/). *GAPDH* and long interspersed nuclear element 1 (LINE-1) were used as endogenous controls for mRNA and genomic DNA levels, respectively.

2.5. RNA interference (RNAi)

For RNAi, small interfering RNA (siRNA) duplex oligoribonucleotides targeting *ARHGAP5* (5′-CAAGATCATAATATCAATCTA-3′) and control (non-silencing) siRNA duplexes were synthesized by QIAGEN (Valencia, CA, USA). The siRNAs were delivered into Huh-7 cells using HiPerfect Transfection Reagent (QIAGEN), according to the manufacturer's protocol.

2.6. Immunoblotting

Immunoblots were prepared according to previously reported methods [7]. Cell lysates (20 μg protein per sample) were separated by sodium dodecyl sulfate-polyacrylamide gel electrophoresis on 10% acrylamide gels. Anti-p190-B RhoGAP monoclonal antibody was obtained from BD Transduction Laboratories (Lexington, KY, USA); anti-RhoA monoclonal antibody was from Santa Cruz Biotechnology (Santa Cruz, CA, USA); and anti-β-actin monoclonal antibody was from Sigma–Aldrich (Tokyo, Japan). For immunoblotting, we used anti-p190-B RhoGAP, anti-RhoA and anti-β-actin at dilutions of 1:250, 1:100 and 1:5000, respectively. For secondary immunodetection, we used anti-mouse IgG (Amersham, Tokyo, Japan) diluted 1:5000. Protein binding was detected using the ECL system (Amersham).

2.7. RhoA activity assay

Active RhoA levels were measured using the enzyme-linked immunosorbent assay (ELISA)-based G-LISA RhoA activation assay Biochem Kit (Cytoskeleton, Denver, CO, USA) according to the manufacturer's instructions. In brief, Huh-7 cells were transfected with siRNA targeting *ARHGAP5* or negative control siRNA, or were left untreated. Cells were then cultured under the standard conditions in DMEM containing 10% FCS. After 48 h, cells were harvested for the RhoA activity assay or trypsinized and held in suspension for 1 h in DMEM containing 1% FCS. The suspended cells were then plated on 6-well plates coated with 5 μg/ml fibronectin (BD Transduction Laboratories) and harvested for the RhoA activity assay at the indicated time points. For the RhoA activity assay, cells were lysed in 70 μl of G-LISA lysis buffer, scraped into tubes and snap frozen in liquid nitrogen. Cell lysates were subsequently thawed, clarified for 2 min at 10,000g, and protein concentrations were normalized between the various time points. Equal amounts of total protein were added to a 96-well plate coated with the Rho-binding domain of Rho effector pro-

teins (which bind active GTP-bound Rho) in triplicate and incubated at 4 °C for 30 min with vigorous shaking. Active Rho levels were determined by subsequent incubations with anti-Rho antibody and secondary horseradish peroxidase-conjugated antibody for 45 min each at room temperature. After adding developing solution, the level of active Rho was determined by measuring absorbance at 490 nm using an ELISA plate reader. Equal loading of total RhoA protein at each time point was determined via immunoblotting using anti-RhoA antibody as described above. Experiments were repeated at least three times.

2.8. Immunofluorescence

Huh-7 cells were transfected with siRNA targeting *ARHGAP5* or negative control siRNA or were left untreated. Cells were harvested 48 h after transfection, suspended for 1 h in DMEM containing 1% FCS and then plated on glass slides coated with fibronectin for 10, 20, 40, 60 or 180 min. Cells were fixed for 10 min in 3.7% formaldehyde, permeabilized for 2 min in 1% Triton X-100 and incubated for 1 h with a blocking buffer (phosphate-buffered saline containing 3% bovine serum albumin). The cells were then incubated for 1 h at room temperature with anti-p190-B RhoGAP monoclonal antibody diluted 1:200 in blocking buffer. Fluorescein isothiocyanate (FITC)-conjugated anti-mouse IgG (Cappel, Aurora, OH, USA) was used to detect the primary antibody. Actin filaments and nuclei were counterstained with rhodamine-phalloidin (Molecular Probes, Eugene, OR, USA) and 4',6-diamidino-2-phenylindole (DAPI; Sigma–Aldrich), respectively.

2.9. Monolayer wound healing assay

Huh-7 cells were transfected with siRNA targeting *ARHGAP5* or negative control siRNA or left untreated. After 24 h, cells in DMEM with 1% FCS were seeded on glass slides coated with fibronectin and allowed to adhere overnight.

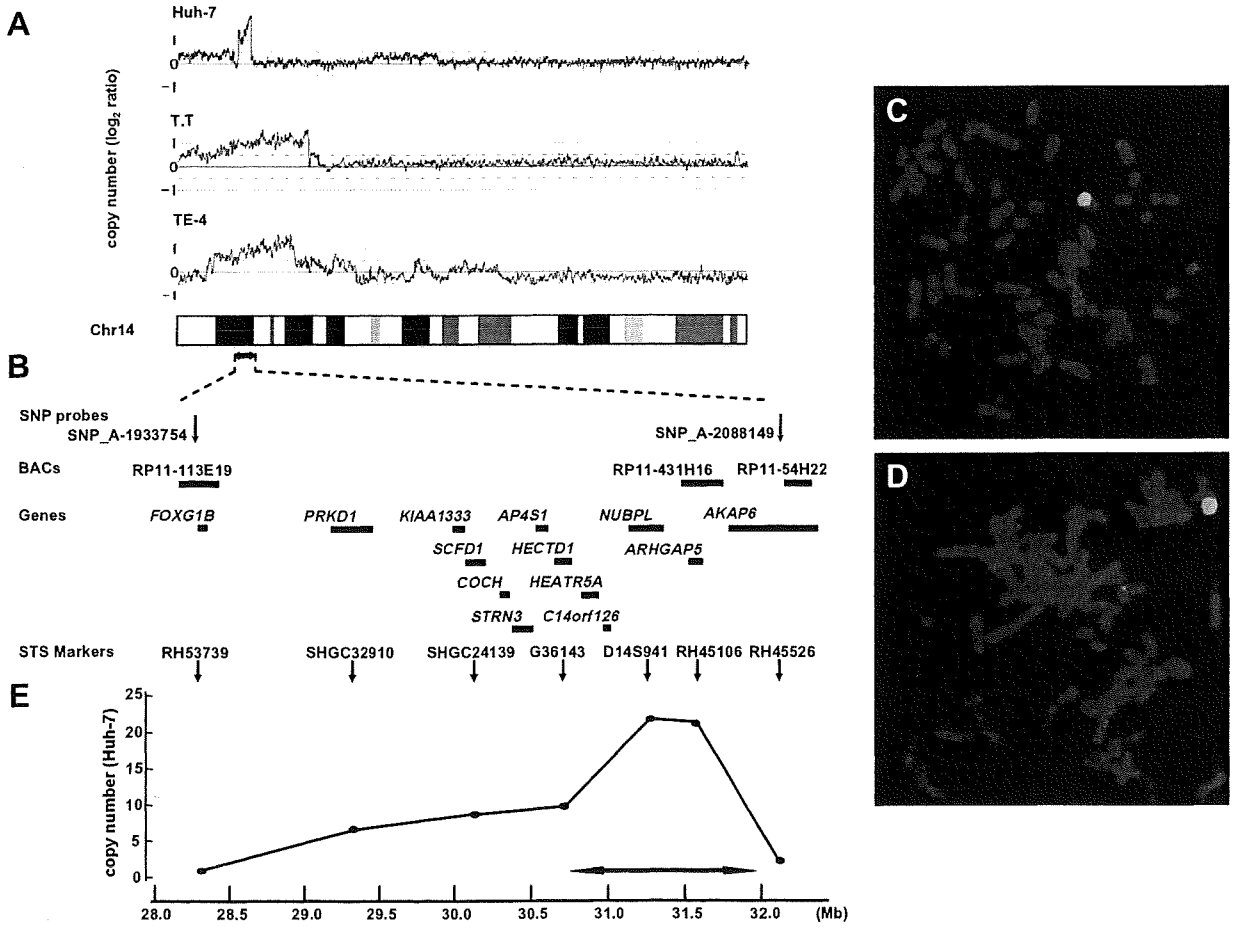

Fig. 1. Map of the amplicon at 14q12. (A) Copy number profiles for chromosome 14 in Huh-7, T.T and TE-4 cells. Copy number values were determined by GeneChip Mapping 250 K array analyses. (B) The positions of the Affymetrix SNP probes, three BACs used as probes for FISH experiments, the 13 genes within the 14q12 amplicon, and the seven STS markers used for real-time quantitative PCR on genomic DNA are shown according to the UCSC genome database (http://genome.ucsc.edu/). (C and D) Representative images of two-color FISH on metaphase chromosomes from Huh-7 cells using BACs: paired RP11-431H16 (green; C) and RP11-113E19 (red; C), or paired RP11-431H16 (green; D) and RP11-54H22 (red; D). (E) Copy numbers at the seven STS marker loci in Huh-7 cells as measured by real-time quantitative PCR with reference to LINE-1 controls. Values are normalized such that the copy number in genomic DNA derived from normal lymphocytes has a value of 2. The smallest region of amplification is indicated (arrow).

We scratched wounds in the cell monolayer using a sterile 200-μl pipet tip, rinsed the cells with phosphate-buffered saline and added DMEM containing 10% FCS with or without mitomycin C (10 μg/ml, Nacalai Tesque, Kyoto, Japan). Cells were allowed to migrate into the wound for 0, 12, or 24 h before fixation. Cells were stained with Giemsa stain (Nacalai Tesque) or were triple-labeled with anti-p190-B RhoGAP, rhodamine-phalloidin and DAPI as described above. Wound widths were measured in three randomly chosen regions. Experiments were repeated at least three times.

2.10. Statistical analysis

Analysis of variance (ANOVA) was performed using SPSS 15.0 software (SPSS Inc., Chicago, IL, USA). *P* values of <0.05 were considered significant.

3. Results

3.1. Detection of 14q12 amplicon in HCC and ESCC cell lines by array analyses

We screened for DNA copy number aberrations in 10 HCC cell lines and 10 ESCC cell lines using GeneChip Mapping 250 K array analysis. Of the 20 cell lines, one HCC cell line, Huh-7, and two ESCC cell lines, T.T and TE-4, commonly exhibited copy number gains at chromosomal region 14q12 (Fig. 1A). In particular, Huh-7 cells showed a high-level gain indicative of amplification in a narrow region on 14q12 between the positions recognized by the Affymetrix SNP_A-1933754 and SNP_A-2088149 probes. To confirm amplification in Huh-7 cells, we performed FISH analyses using BACs RP11-113E19, RP11-431H16 and RP11-54H22 as probes (Fig. 1B–D). BAC RP11-431H16 generated strong signals as a small homogeneously staining region (HSR), indicating amplification (Figs. 1C, D). In contrast, BACs RP11-113E19 or RP11-54H22 did not show a HSR pattern, indicating their positions outside the amplicon (Fig. 1C and D). Furthermore, we determined gene dosages in Huh-7 cells at the STS markers RH53739, SHGC32910, SHGC24139, G36143, D14S941, RH45106, and RH45526 loci by real time quantitative PCR. (Fig.1B and E). The highest copy number was observed at the D14S941 and RH45106 loci. Taken together, we defined the smallest region of amplification between markers G36143 and RH45526. The extent of the amplicon was estimated to be 1.2 Mb. This region includes four known or predicted protein-coding genes, *HEATR5A*, *c14orf126*, *NUBPL*, and *ARHGAP5*.

3.2. Identification of candidate target genes in the 14q12 amplicon

The 14q12 region may harbor one or more genes (henceforth called 'target genes') that, when activated by amplification, play a role in carcinogenesis. A common criterion for designating a gene as a putative target is that amplification leads to its overexpression [8]. Using real-time quantitative PCR, we determined mRNA levels of all four genes within the amplicon in the 10 HCC cell lines and 10 ESCC cell lines. Among the four genes, *HEATR5A* and *ARHGAP5* were commonly overexpressed in Huh-7, T.T and TE-4 cells, the cell lines that were found to have copy number gains at 14q12 (Fig. 2A). These findings identified *ARHGAP5*, which encodes p190-B RhoGAP, as one of candidate target genes for the 14q12 amplicon.

We determined copy numbers of *ARHGAP5* in the 10 HCC and 10 ESCC cell lines by real-time quantitative PCR (Fig. 2B). Copy number changes were counted as gains if the results of the analysis for a given tumor cell type exceeded the twofold levels of the gene in normal cells. A copy number gain of *ARHGAP5* was observed in six (30%) of the 20 cell lines: Huh-7, T.T, KYSE140, TE-4, TE-6 and TE-10.

We examined the expression of p190-B RhoGAP protein in 4 HCC and 4 ESCC cell lines by immunoblot analysis. As shown in Fig. 2C, expression levels of p190-B RhoGAP were higher in cell lines exhibiting copy number gains of *ARHGAP5* (Huh-7, T.T, KYSE140, TE-4 and TE-10) than other cell lines that did not show gains (SNU354, Huh-1 and PLC/PRF/5).

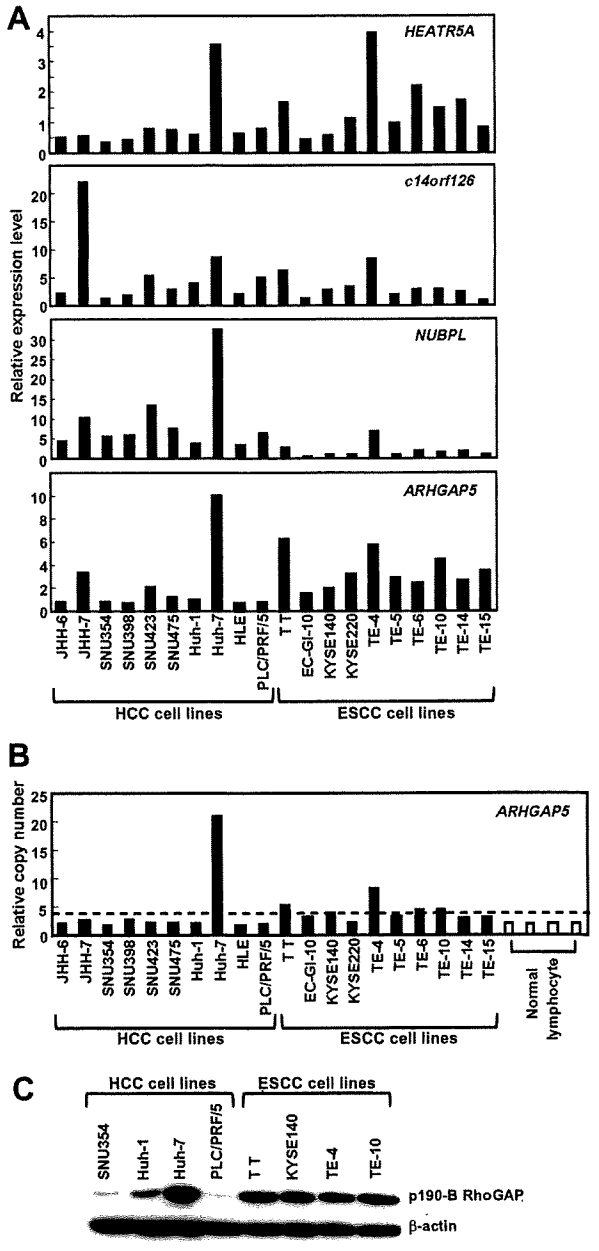

Fig. 2. Amplification and overexpression of *ARHGAP5* in Huh-7, T.T and TE-4 cell lines. (A) Relative expression levels of four genes (*HEATR5A*, *c14orf126*, *NUBPL* and *ARHGAP5*) within the 14q12 amplicon in 10 HCC and 10 ESCC cell lines as evaluated by real-time quantitative PCR. Results are presented as expression levels of each gene relative to a reference gene (*GAPDH*) to correct for variations in the amount of RNA. (B) Copy numbers at the *ARHGAP5* locus (the STS marker RH45106) in 10 HCC cell lines, 10 ESCC cell lines and four normal peripheral blood lymphocytes as measured by real-time quantitative PCR with reference to LINE-1 controls. Values are normalized such that the average copy number in genomic DNA derived from four normal lymphocytes has a value of 2. A value of 4, which is a twofold increase in copy number of normal lymphocytes, was used to determine the cut-off value for copy number gain, shown as a dotted line. (C) Levels of p190-B RhoGAP and β-actin, an internal control, determined by immunoblotting in 4 HCC and 4 ESCC cell lines.

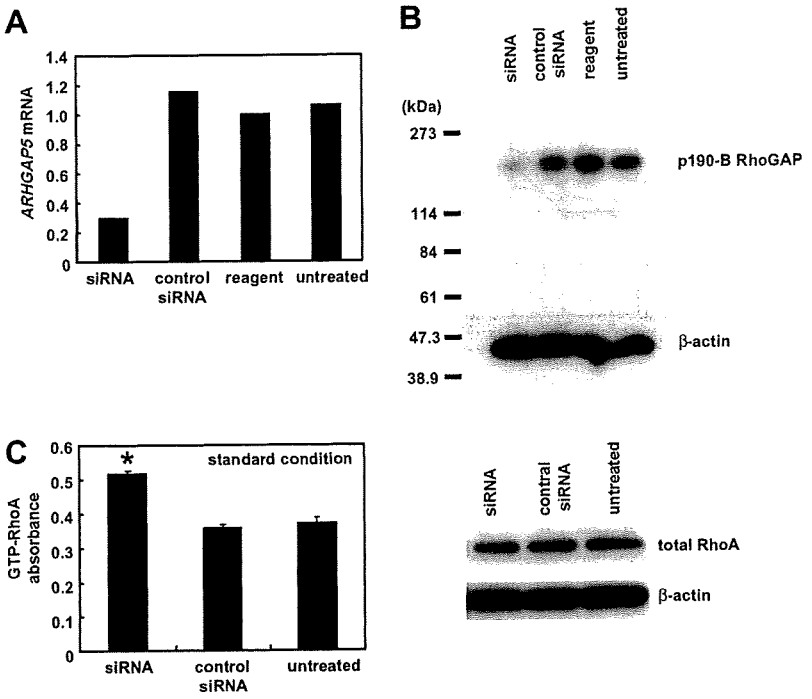

Fig. 3. Knockdown of *ARHGAP5* increases RhoA activity. (A) Relative expression levels of *ARHGAP5* mRNA as determined by real-time quantitative PCR. Huh-7 cells were treated with siRNA targeting *ARHGAP5*, negative control siRNA or transfection agent alone. Untreated cells were maintained under identical experimental conditions. Results are presented as a ratio between the expression level of *ARHGAP5* and that of a reference gene (*GAPDH*) to correct for variation in the amount of RNA. Relative expression levels were normalized such that the ratio in untreated cells was 1. (B) Levels of p190-B RhoGAP and β-actin, an internal control, determined by immunoblotting. (C) (*left*) Levels of RhoA activity under standard culture conditions (DMEM containing 10% FCS). RhoA activity was measured using a G-LISA kit (see Methods section). Values are represented as the mean ± S.D. Differences were analyzed by ANOVA ($^*P < 0.05$). (*right*) Total RhoA and β-actin were determined by immunoblotting.

3.3. Regulation of RhoA activity by p190-B RhoGAP in Huh-7 cells

To investigate the biological function of p190-B RhoGAP in HCC cells, knockdown of *ARHGAP5* expression in Huh-7 cells was carried out using RNAi. Following treatment of Huh-7 cells with siRNA targeting *ARHGAP5*, we observed a decrease in both *ARHGAP5* mRNA and p190-B RhoGAP protein levels relative to what was observed for cells receiving control siRNA, transfection agent alone or left untreated (Fig. 3A and B). Because p190-B RhoGAP negatively regulates RhoA activity, we examined the effect of the siRNA-mediated knockdown of *ARHGAP5* on RhoA activity. Huh-7 cells were treated with *ARHGAP5* siRNA or control siRNA or were left untreated. Cells were then cultured in DMEM containing 10% FCS for 48 h under standard conditions. RhoA activity levels were higher in cells treated with *ARHGAP5* siRNA than in cells treated with control siRNA or in untreated cells, whereas total RhoA levels were similar among the three groups (Fig. 3C). These findings suggest that overexpression of *ARHGAP5* contributes to downregulation of RhoA activity in Huh-7 cells.

3.4. Regulation of cell spreading by p190-B RhoGAP in Huh-7 cells

It is known that integrin-mediated adhesion regulates the activity of p190-B RhoGAP and RhoA [3,9]. We therefore examined the function of p190-B RhoGAP when Huh-7 cells were plated on fibronectin, a specific ligand for α5β1 integrin. Huh-7 cells treated with *ARHGAP5* siRNA or control siRNA or left untreated were suspended and plated on fibronectin. Prior to and during plating, cells were maintained in DMEM containing 1% FCS. Adhesion to fibronectin regulated RhoA activity in a triphasic or biphasic manner (Fig. 4A). Prior to plating (0 min), RhoA activity was significantly higher in *ARHGAP5* siRNA-treated cells than in control siRNA-treated cells or untreated cells. In *ARHGAP5* siRNA-treated cells, RhoA activity rapidly and transiently decreased (20 min). This initial decline was followed by an increase that peaked at 60 min. In the final phase, RhoA activity gradually decreased. In control siRNA-treated cells or untreated cells, an initial period of low RhoA activity was followed by a slight increase that peaked between 40–60 min and then returned to basal level. RhoA activity was significantly higher in *ARHGAP5* siRNA-treated cells than control siRNA-treated cells or untreated cells between 40 and 180 min. During the experimental period, expression of p190-B RhoGAP was continuously knocked down by *ARHGAP5* siRNA and total RhoA levels were similar among the three groups (Fig. 4A).

Because RhoA affects cell motility by stimulating reorganization of actin, we examined whether p190-B RhoGAP regulates the spreading of Huh-7 cells on fibronectin. Using immunofluorescence, we observed morphological changes in Huh-7 cells during attachment and spreading on fibronectin (Fig. 4B). Phalloidin staining revealed that *ARHGAP5* siRNA-treated cells exhibited more robust actin stress fibers but less membrane ruffling and protrusion at the cell periphery than control siRNA-treated cells or untreated cells. The actin stress fiber formation and reduced membrane ruffling and protrusion observed in *ARHGAP5* siRNA-treated cells corresponded with higher RhoA activity (Fig. 4)

p190-B RhoGAP was expressed diffusely in the cytoplasm of control siRNA-treated cells and untreated cells, whereas it was hardly detected in *ARHGAP5* siRNA-treated cells. We found that p190-B RhoGAP had partially translocated to the membrane protrusions in control siRNA-treated cells and untreated cells by 40 min after plating (Fig. 4B). Taken together, these findings suggest that RhoA inactivation by p190-B RhoGAP results in inhibition of actin stress fiber formation, enhanced membrane ruffling and protrusion and promotion of cell spreading on fibronectin.

3.5. Regulation of cell migration by p190-B RhoGAP in Huh-7 cells

To investigate the role of p190-B RhoGAP in cell motility, we performed a monolayer wound healing assay. Wound closure was delayed in *ARHGAP5* siRNA-treated cells relative to control siRNA-treated cells or untreated cells, whether cultured in the presence of mitomycin C or in its absence (Figs. 5A–E). Mitomycin C blocks mitosis and thus allows analysis of cell migration in the absence of cell proliferation. These results show that cell migration, rather than cell proliferation, is the major factor

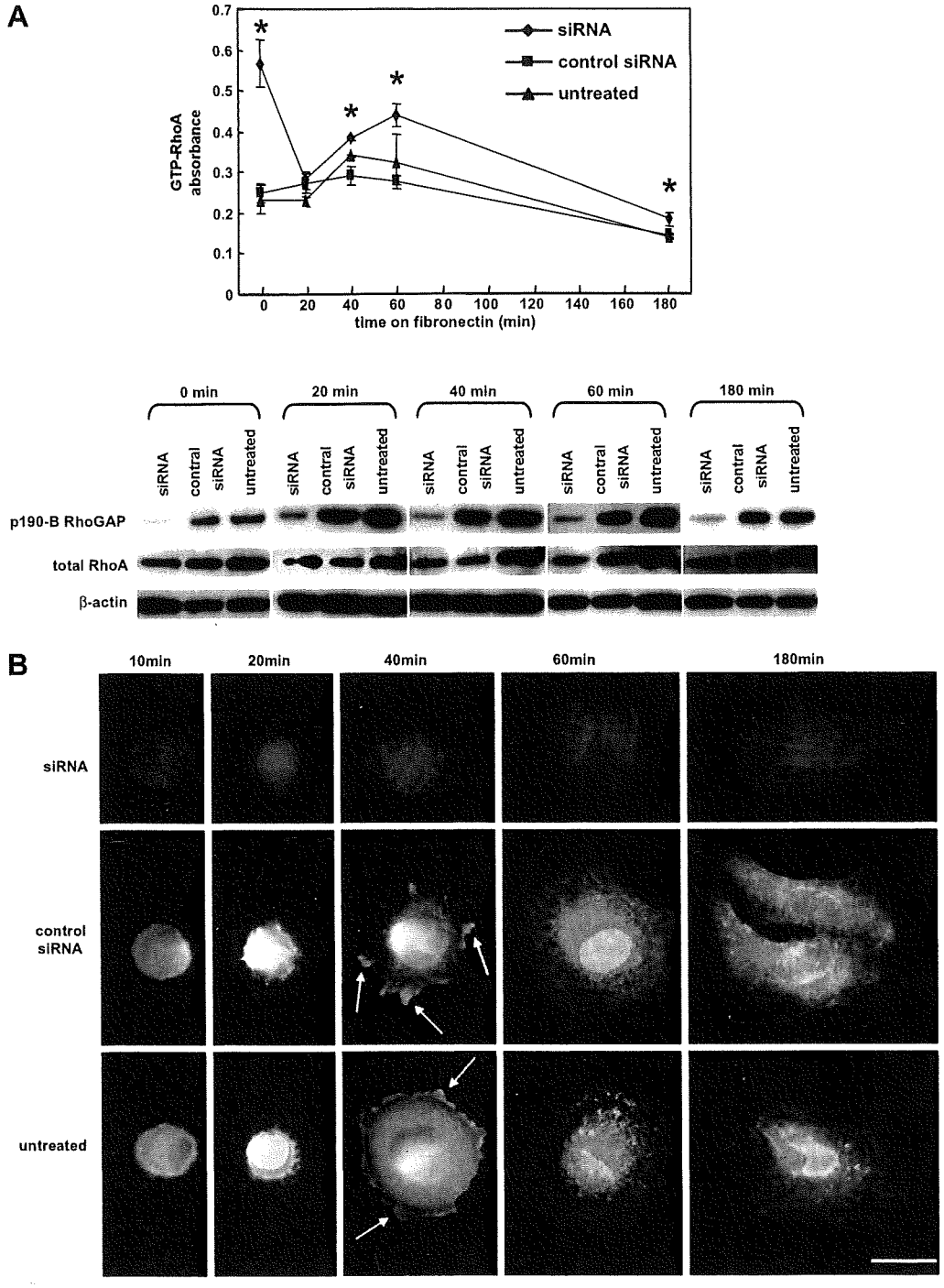

Fig. 4. Knockdown of *ARHGAP5* inhibits Huh-7 cell spreading on fibronectin. (A) Time course of changes in RhoA activity (*upper*) and levels of p190-B RhoGAP and total RhoA (*lower*). Huh-7 cells treated with siRNA targeting *ARHGAP5* or control siRNA or left untreated were plated on fibronectin as described in Materials and Methods and harvested at the indicated time points. Values of RhoA activity are represented as the mean ± SD. Differences were analyzed by ANOVA ($^{*}P < 0.05$). Levels of p190-B RhoGAP, total RhoA and β-actin were determined by immunoblotting. (B) Time course of cell spreading on fibronectin. Huh-7 cells treated with siRNA targeting *ARHGAP5* or control siRNA or left untreated were plated on fibronectin, fixed at the indicated time points and then triple-labeled with anti-p190-B RhoGAP, rhodamine-conjugated phalloidin and DAPI to reveal p190-B RhoGAP (green), actin filaments (red), and nuclei (blue), respectively. Arrows indicate p190-B RhoGAP on membrane protrusions. Scale bar = 10 μm.

in the retarded wound repair process in *ARHGAP5* siRNA-treated cells. Wound edge cells in *ARHGAP5* siRNA-treated cells had more abundant actin stress fibers but less membrane ruffling and protrusion at the leading edge than control siRNA-treated or untreated cells (Figs. 5F–H). p190-B RhoGAP translocated to the membrane protrusions of control siRNA-treated or untreated cells at the edge of the wound, but not in *ARHGAP5*-siR-

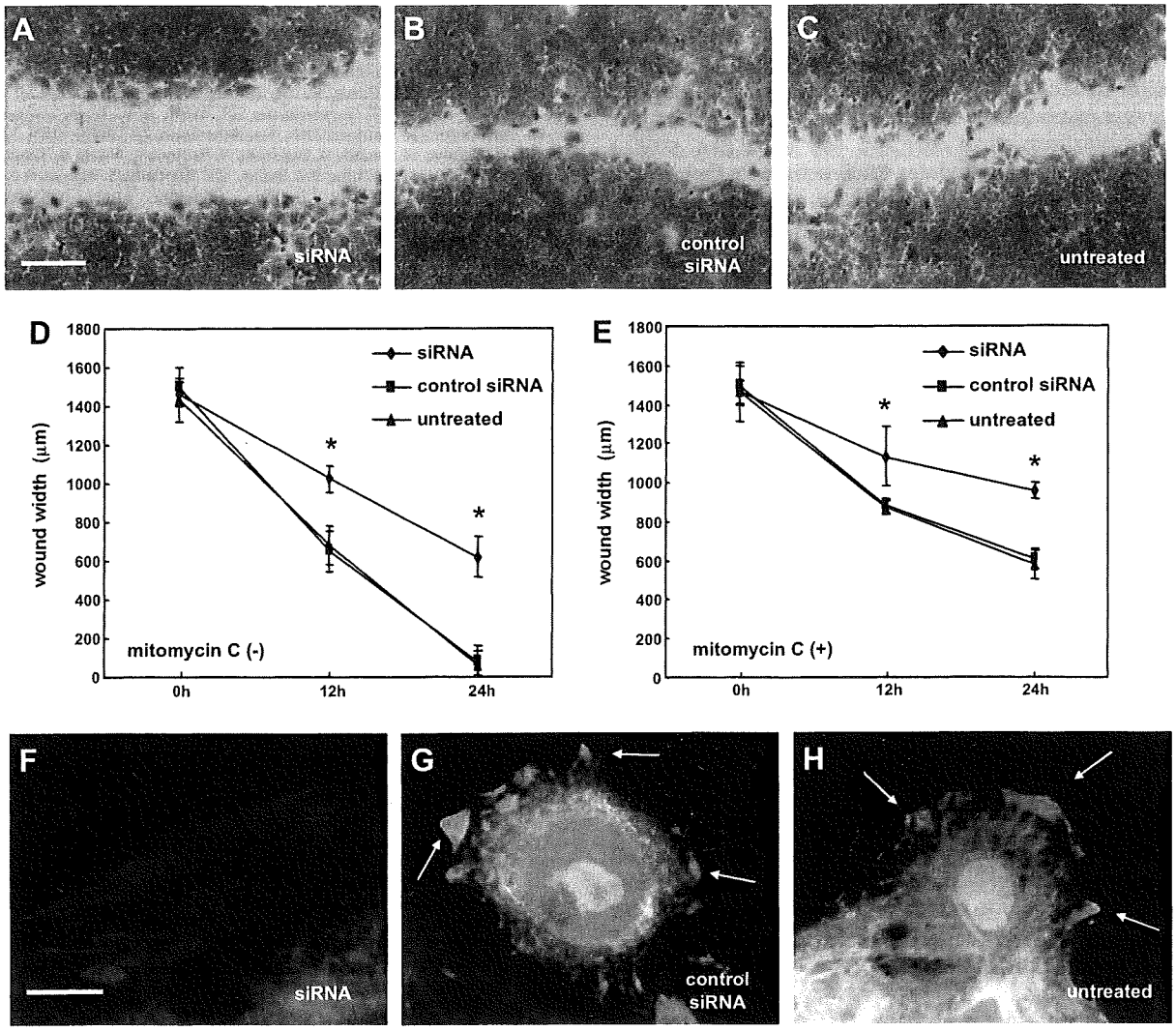

Fig. 5. Knockdown of *ARHGAP5* inhibits migration in Huh-7 cells. Monolayer wound healing assay in Huh-7 cells transfected with siRNA targeting *ARHGAP5* (A, F) or control siRNA (B and G), or left untreated (C and H). Cells were cultured in the absence (A–D, F–H) or presence (E) of mitomycin C. (A–C) Cells were allowed to migrate into a monolayer wound for 24 h and afterward stained with Giemsa stain. Original magnifications: 40×. Scale bar = 500 μm. (D and E) Cells were cultured in the absence (D) or presence (E) of mitomycin C. Wound widths were measured in three randomly chosen regions at the indicated time after wounding. Values are represented as the mean ± SD. Differences were analyzed by ANOVA ($^{*}P < 0.05$). (F–H) Wound edge cells were triple-labeled with anti-p190-B RhoGAP, rhodamine-conjugated phalloidin and DAPI to reveal p190-B RhoGAP (green), actin filaments (red) and nuclei (blue), respectively. Arrows indicate p190-B RhoGAP on membrane protrusions. Scale bar = 10 μm.

NA cells. Taken together, these observations suggest that the inhibition of RhoA activity by p190-B RhoGAP promotes cell movement and formation of membrane protrusions in migrating cells.

4. Discussion

We report here the amplification of *ARHGAP5* in HCC and ESCC cell lines. We undertook a molecular definition of the amplicon at 14q12 that is present in HCC and ESCC cell lines. The amplification at 14q12 has been reported in various types of cancers, including HCC [10], ESCC [7], nasopharyngeal carcinoma [11] and non-squamous cell lung carcinoma [12], although the frequency of 14q12 gain is low in primary HCC (4–6%) [10,13]. The range of the amplicon varies among these tumors, and their boundaries have not been determined in each case. Moreover, the target oncogene(s) in the amplified regions have not been fully identified. Here we defined the amplified regions in one HCC and two ESCC cell lines and narrowed the site of the amplification to a relatively short section. Among the four genes within the smallest region of the amplification, only *HEATR5A* and *ARHGAP5* were overexpressed in all the tested lines exhibiting copy number gains in the region; hence they are thought to be candidate targets in the amplicon. Of the two genes, we chose to focus further analysis on *ARHGAP5* because its protein product, p190-B RhoGAP, is purported to play an important role in dynamic cellular processes by regulating RhoA activity, while little is known about *HEATR5A*. During the preparation of this manuscript, amplification of *ARHGAP5* was reported in Huh-7 cells [14].

Although several studies have suggested an association of p190-B RhoGAP with tumors [15–17], its biological function in cancer cells is poorly understood. Therefore, using siRNA, we studied its function in Huh-7 cells; the HCC cell line that exhibited the most remarkable copy number gain and overexpression of *ARHGAP5*. We found that p190-B RhoGAP negatively regulates RhoA activity in Huh-7 cells cultured in medium containing 10% FCS and plated on fibronectin. Adhesion to fibronectin regulated RhoA activity in a triphasic or biphasic manner, as previously reported in fibroblasts [18,19]. Although some RhoA activity is required for migration, possibly to maintain sufficient adhesion to the substrate, high activity inhibits movement [19–22]. Our results showed that RhoA inactivation by p190-B RhoGAP results in inhibition of actin stress fiber formation, enhanced membrane ruffling and protrusion, and promotion of spreading and migration of Huh-7 cells. These findings are in agreement with results obtained from previous studies. A dominant negative (loss-of-function) p190-B RhoGAP mutation elevates RhoA activity in fibroblasts cultured on fibronectin and inhibits their migration, whereas overexpression of wild-type p190-B RhoGAP decreases RhoA activity, promotes the formation of membrane protrusions and enhances mobility [19]. Activation of β1 integrin signaling stimulates tyrosine phosphorylation of p190-B RhoGAP and promotes membrane protrusion at invadopodia in a melanoma cell line [17]. p190-B RhoGAP is also involved in invasion by breast cancer cells [15].

In conclusion, we have identified *ARHGAP5* as a probable target for the amplification at 14q12 detected in a subgroup of HCCs and ESCCs. Our results indicate that p190-B RhoGAP, the protein product of *ARHGAP5*, promotes cell spreading and migration in Huh-7 cells. Further studies are needed to determine the importance of *ARHGAP5* and p190-B RhoGAP in the development and progression of not only HCC and ESCC but also other types of tumors.

Conflicts of interest statement

My co-authors and I declare that we have no proprietary, financial, professional or other personal interest of any nature or kind in any product, service and/or company that could be construed as influencing the position presented in the manuscript entitled, "A novel amplification target, ARHGAP5, promotes cell spreading and migration by negatively regulating RhoA in Huh-7 hepatocellular carcinoma cells".

Acknowledgements

Supported by: Grants-in-Aid for Scientific Research (18390223) from the Japan Society for the Program of Science (to K.Yasui).

References

[1] A. Hall, Rho GTPases and the actin cytoskeleton, Science 279 (1998) 509–514.
[2] P.D. Burbelo, S. Miyamoto, A. Utani, S. Brill, K.M. Yamada, A. Hall, Y. Yamada, P190-B, a new member of the Rho GAP family, and Rho are induced to cluster after integrin cross-linking, J. Biol. Chem. 270 (1995) 30919–30926.
[3] W.T. Arthur, L.A. Petch, K. Burridge, Integrin engagement suppresses RhoA activity via a c-Src-dependent mechanism, Curr. Biol. 10 (2000) 719–722.
[4] G.C. Kennedy, H. Matsuzaki, S. Dong, W.N. Liu, J. Huang, G. Liu, X. Su, M. Cao, W. Chen, J. Zhang, W. Liu, G. Yang, X. Di, T. Ryder, Z. He, U. Surti, M.S. Phillips, M.T. Boyce-Jacino, S.P. Fodor, K.W. Jones, Large-scale genotyping of complex DNA, Nat. Biotechnol. 21 (2003) 1233–1237.
[5] Y. Nannya, M. Sanada, K. Nakazaki, N. Hosoya, L. Wang, A. Hangaishi, M. Kurokawa, S. Chiba, D.K. Bailey, G.C. Kennedy, S. Ogawa, A robust algorithm for copy number detection using high-density oligonucleotide single nucleotide polymorphism genotyping arrays, Cancer Res. 65 (2005) 6071–6079.
[6] Y. Inagaki, K. Yasui, M. Endo, T. Nakajima, K. Zen, K. Tsuji, M. Minami, S. Tanaka, M. Taniwaki, Y. Itoh, S. Arii, T. Okanoue, CREB3L4, INTS3, and SNAPAP are targets for the 1q21 amplicon frequently detected in hepatocellular carcinoma, Cancer Genet. Cytogenet. 180 (2008) 30–36.
[7] K. Yasui, I. Imoto, Y. Fukuda, A. Pimkhaokham, Z.Q. Yang, T. Naruto, Y. Shimada, Y. Nakamura, J. Inazawa, Identification of target genes within an amplicon at 14q12–q13 in esophageal squamous cell carcinoma, Genes Chromosomes Cancer 32 (2001) 112–118.
[8] C. Collins, J.M. Rommens, D. Kowbel, T. Godfrey, M. Tanner, S.I. Hwang, D. Polikoff, G. Nonet, J. Cochran, K. Myambo, K.E. Jay, J. Froula, T. Cloutier, W.L. Kuo, P. Yaswen, S. Dairkee, J. Giovanola, G.B. Hutchinson, J. Isola, O.P. Kallioniemi, M. Palazzolo, C. Martin, C. Ericsson, D. Pinkel, D. Albertson, W.B. Li, J.W. Gray, Positional cloning of ZNF217 and NABC1: genes amplified at 20q13.2 and overexpressed in breast carcinoma, Proc. Natl. Acad. Sci. USA 95 (1998) 8703–8708.
[9] E.A. Cox, S.K. Sastry, A. Huttenlocher, Integrin-mediated adhesion regulates cell polarity and membrane protrusion through the Rho family of GTPases, Mol. Biol. Cell 12 (2001) 265–277.
[10] C. Sakakura, A. Hagiwara, H. Taniguchi, T. Yamaguchi, H. Yamagishi, T. Takahashi, K. Koyama, Y. Nakamura, T. Abe, J. Inazawa, Chromosomal aberrations in human hepatocellular carcinomas associated with hepatitis C virus infection detected by comparative genomic hybridization, Br. J. Cancer 80 (1999) 2034–2039.
[11] Y.J. Chen, J.Y. Ko, P.J. Chen, C.H. Shu, M.T. Hsu, S.F. Tsai, C.H. Lin, Chromosomal aberrations in nasopharyngeal carcinoma analyzed by comparative genomic hybridization, Genes Chromosomes Cancer 25 (1999) 169–175.
[12] T. Yakut, H.J. Schulten, A. Demir, D. Frank, B. Danner, U. Egeli, C. Gebitekin, E. Kahler, B. Gunawan, N. Urer, H. Oztürk, L. Füzesi, Assessment of molecular events in squamous and non-squamous cell lung carcinoma, Lung Cancer 54 (2006) 293–301.
[13] P. Moinzadeh, K. Breuhahn, H. Stützer, P. Schirmacher, Chromosome alterations in human hepatocellular carcinomas correlate with aetiology and histological grade – results of an explorative CGH meta-analysis, Br. J. Cancer 92 (2005) 935–941.
[14] C. Schlaeger, T. Longerich, C. Schiller, P. Bewerunge, A. Mehrabi, G. Toedt, J. Kleeff, V. Ehemann, R. Eils, P. Lichter, P. Schirmacher, B. Radlwimmer, Etiology-dependent molecular mechanisms in human hepatocarcinogenesis, Hepatology 47 (2008) 511–520.
[15] S. Zrihan-Licht, Y. Fu, J. Settleman, K. Schinkmann, L. Shaw, I. Keydar, S. Avraham, H. Avraham, RAFTK/Pyk2 tyrosine kinase mediates the association of p190 RhoGAP with RasGAP and is involved in breast cancer cell invasion, Oncogene 19 (2000) 1318–1328.
[16] G. Chakravarty, D. Roy, M. Gonzales, J. Gay, A. Contreras, J.M. Rosen, P190-B, a Rho-GTPase-activating protein, is differentially expressed in terminal end buds and breast cancer, Cell Growth Differ. 11 (2000) 343–354.
[17] H. Nakahara, S.C. Mueller, M. Nomizu, Y. Yamada, Y. Yeh, W.T. Chen, Activation of beta1 integrin signaling stimulates tyrosine phosphorylation of p190RhoGAP and membrane-protrusive activities at invadopodia, J. Biol. Chem. 273 (1998) 9–12.
[18] X.D. Ren, W.B. Kiosses, M.A. Schwartz, Regulation of the small GTP-binding protein Rho by cell adhesion and the cytoskeleton, EMBO J. 18 (1999) 578–585.
[19] W.T. Arthur, K. Burridge, RhoA inactivation by p190RhoGAP regulates cell spreading and migration by promoting membrane protrusion and polarity, Mol. Biol. Cell 12 (2001) 2711–2720.
[20] K. Takaishi, T. Sasaki, M. Kato, W. Yamochi, S. Kuroda, T. Nakamura, M. Takeichi, Y. Takai, Involvement of Rho p21 small GTP-binding protein and its regulator in the HGF-induced cell motility, Oncogene 9 (1994) 273–279.
[21] A.J. Ridley, P.M. Comoglio, A. Hall, Regulation of scatter factor/hepatocyte growth factor responses by Ras, Rac, and Rho in MDCK cells, Mol. Cell. Biol. 15 (1995) 1110–1122.
[22] C.D. Nobes, A. Hall, Rho GTPases control polarity, protrusion, and adhesion during cell movement, J. Cell Biol. 144 (1999) 1235–1244.

GENES, CHROMOSOMES & CANCER 48:109–120 (2009)

RESEARCH ARTICLES

ERK5 is a Target for Gene Amplification at 17p11 and Promotes Cell Growth in Hepatocellular Carcinoma by Regulating Mitotic Entry

Keika Zen,[1] Kohichiroh Yasui,[1]* Tomoaki Nakajima,[1] Yoh Zen,[2] Kan Zen,[3] Yasuyuki Gen,[1] Hironori Mitsuyoshi,[1] Masahito Minami,[1] Shoji Mitsufuji,[1] Shinji Tanaka,[4] Yoshito Itoh,[1] Yasuni Nakanuma,[2] Masafumi Taniwaki,[5] Shigeki Arii,[4] Takeshi Okanoue,[1] and Toshikazu Yoshikawa[1]

[1]Molecular Gastroenterology and Hepatology, Graduate School of Medical Science, Kyoto Prefectural University of Medicine, Kyoto, Japan
[2]Department of Human Pathology, Kanazawa University Graduate School of Medicine, Kanazawa, Japan
[3]Division of Cardiovascular Medicine, Omihachiman Community Medical Center, Omihachiman, Japan
[4]Department of Hepato-Biliary-Pancreatic Surgery, Tokyo Medical and Dental University, Tokyo, Japan
[5]Molecular Hematology and Oncology, Graduate School of Medical Science, Kyoto Prefectural University of Medicine, Kyoto, Japan

Using high-density oligonucleotide microarrays, we investigated DNA copy-number aberrations in cell lines derived from hepatocellular carcinomas (HCCs) and detected a novel amplification at 17p11. To identify the target of amplification at 17p11, we defined the extent of the amplicon and examined HCC cell lines for expression of all seven genes in the 750-kb commonly amplified region. Mitogen-activated protein kinase (MAPK) 7, which encodes extracellular-regulated protein kinase (ERK) 5, was overexpressed in cell lines in which the gene was amplified. An increase in *MAPK7* copy number was detected in 35 of 66 primary HCC tumors. Downregulation of *MAPK7* by small interfering RNA suppressed the growth of SNU449 cells, the HCC cell line with the greatest amplification and overexpression of *MAPK7*. ERK5, phosphorylated during the G2/M phases of the cell cycle, regulated entry into mitosis in SNU449 cells. In conclusion, our results suggest that *MAPK7* is likely the target of 17p11 amplification and that the ERK5 protein product of *MAPK7* promotes the growth of HCC cells by regulating mitotic entry.

INTRODUCTION

Hepatocellular carcinoma (HCC) is the fifth most common malignancy in the world and is estimated to cause approximately half a million deaths annually (El-Serag, 2002). Several risk factors for HCC have been reported, including infection with hepatitis B and C viruses, dietary intake of afratoxin, alcohol consumption, and diabetes.

The mitogen-activated protein kinase (MAPK) cascades transmit extracellular signals from cell surface receptors to specific intracellular targets and regulate a wide variety of cellular functions, including cell proliferation, differentiation, and the stress response (Nishimoto and Nishida, 2006). Extracellular stimuli induce sequential activation of MAPK kinase kinase, MAPK kinase, and MAPK. At least four MAPK subfamilies have been identified: extracellular-regulated protein kinase (ERK) 1 and 2, c-Jun-N-terminal kinases, p38, and ERK5 (also know as BMK1). ERK5, which was recently characterized, can be activated by a wide range of growth factors and cellular stresses, including serum, epithelial growth factor, oxidative stress, and hyperosmotic shock (Hayashi and Lee, 2004; Nishimoto and Nishida, 2006; Wang and Tournier, 2006). When stimulated, MAP/ERK kinase kinase 2 and 3 activate MAP/ERK kinase (MEK) 5, a specific kinase for ERK5. Subsequently, MEK5 phosphorylates ERK5, and the activated ERK5 promotes cell proliferation, differentiation, and survival (Hayashi and Lee, 2004; Garaude et al., 2006; Nishimoto and Nishida, 2006; Wang and Tournier, 2006). Some investigators have described the possible involvement of ERK5 in cancers (Esparis-Ogando et al., 2002; Weldon et al., 2002; Mulloy et al., 2003; Carvajal-Vergara et al., 2005; Linnerth et al., 2005).

Additional Supporting Information may be found in the online version of this article.

Supported by: Grants-in-Aid for Scientific Research from the Japan Society for the Program of Science, Grant number: 18390223.

*Correspondence to: Kohichiroh Yasui, Molecular Gastroenterology and Hepatology, Graduate School of Medical Science, Kyoto Prefectural University of Medicine, 465 Kajii-cho, Kamigyo-ku, Kyoto, 602-8566, Japan. E-mail: yasuik@koto.kpu-m.ac.jp

Received 24 May 2008; Accepted 11 September 2008
DOI 10.1002/gcc.20624
Published online 30 October 2008 in Wiley InterScience (www.interscience.wiley.com).

Accumulating evidence suggests that multiple sequential genetic alterations in a cell lineage at the nucleotide and chromosome levels underlie the carcinogenesis of solid tumors. Amplification of chromosomal DNA is one mechanism of activating genes whose overexpression contributes to the development and progression of cancer. Regions of chromosomal amplification in cancer cells frequently harbor oncogenes, such as *MYC* (Little et al., 1983) and *ERBB2* (Di Fiore et al., 1987). Using comparative genomic hybridization (CGH), we have detected novel regions of amplification in a variety of cancer types, including HCC, and we have identified a number of candidate oncogenes from amplicons (Yasui et al., 2001; Yasui et al., 2002; Yokoi et al., 2002; Okamoto et al., 2003; Yokoi et al., 2003). CGH was initially used for genome-wide detection of copy number changes occurring in cancers (Kallioniemi et al., 1992). However, its resolution is limited (5–10 Mb) because it detects segmental copy number changes on metaphase chromosomes.

The recent introduction of high-density oligonucleotide microarrays designed for typing of single nucleotide polymorphisms (SNPs) facilitates high-resolution mapping of chromosomal amplifications, deletions, and loss of heterozygosity (Mei et al., 2000; Bignell et al., 2004; Matsuzaki et al., 2004a,b; Wong et al., 2004; Zhao et al., 2004). The Affymetrix GeneChip Mapping 100K array set contains 116,204 SNP loci with a mean intermarker distance of 23.6 kb, and it enables detailed and genome-wide identification of DNA copy number changes (Matsuzaki et al., 2004a,b; Garraway et al., 2005; Zhao et al., 2005). The newer GeneChip Mapping 500K array set is composed of two arrays, each capable of genotyping an average 250,000 SNPs.

In the work reported here, we investigated DNA copy number aberrations in HCC cell lines using Affymetrix high-density SNP arrays. We identified a novel amplification at 17p11 in HCC cell lines. This region may harbor one or more genes that, when amplified, contribute to carcinogenesis. Within the amplicon, *MAPK7*, which encodes ERK5, emerged as a probable target gene that acts as a driving force for amplification of the region and promotes the growth of HCC cells by regulating entry into mitosis.

MATERIALS AND METHODS

Cell Lines and Tumor Samples

A total of 21 liver cancer cell lines [HCC-derived HLE, HLF (Dor et al., 1975), PLC/PRF/5 (Alexander et al., 1976), Li7 (Hirohashi et al., 1979), Huh7 (Nakabayashi et al., 1982), Hep3B (Aden et al., 1979), SNU354, SNU368, SNU387, SNU398, SNU423, SNU449, SNU475 (Park et al., 1995), JHH-1, JHH-2, JHH-4, JHH-5, JHH-6, JHH-7 (Fujise et al., 1990), Huh-1 (Huh et al., 1981), and the hepatoblastoma line HepG2 (Knowles et al., 1980)] were examined in this study. All cell lines were maintained in Dulbecco's modified Eagle's medium supplemented with 10% fetal bovine serum. We obtained 66 primary HCC tumors for analysis of the DNA copy number of *MAPK7* from patients undergoing surgery at the hospitals of Tokyo Medical and Dental University and Kyoto University, Japan. Genomic DNA was isolated from each cell line and from 66 primary tumors using the Puregene DNA isolation kit (Gentra, Minneapolis, MN). For immunohistochemical studies of ERK5, 43 additional HCC samples were obtained from the Hospital of Kyoto Prefectural University of Medicine, Japan. Before initiation of the present study, informed consent was obtained in the formal style approved by all relevant ethical committees.

SNP Assay

The GeneChip Mapping 100K array set and GeneChip Mapping 250K Sty array (Affymetrix, Santa Clara, CA) were used in this study. Analyses were performed according to the manufacturer's instructions. In brief, 250 ng of genomic DNA was digested with a restriction enzyme (*Xba*I or *Hind*III for the 100K array set and *Sty*I for the 250K Sty array), ligated to an adaptor, and amplified by PCR (Kennedy et al., 2003; Matsuzaki et al., 2004a,b; Zhao et al., 2004). Amplified products were fragmented, labeled by biotinylation, and hybridized to the microarrays. Hybridization was detected by incubation with a streptavidin-phycoerythrin conjugate, followed by scanning of the array, and analysis was performed as described previously (Kennedy et al., 2003; Di et al., 2005). Copy number changes were calculated using the Copy Number Analyzer for Affymetrix GeneChip Mapping Arrays (http://www.genome.umin.jp) (Nannya et al., 2005).

Fluorescence In Situ Hybridization

We performed FISH using the bacterial artificial chromosome (BAC) RP11-73E4 as a probe (Invitrogen, Carlsbad, CA) as described previously (Yasui et al., 2002). The BAC was selected

on the basis of its location according to the database provided by the UCSC (http://genome.ucsc.edu/). Briefly, the probe was labeled by nick translation with biotin-16-dUTP (Roche Diagnostics, Penzberg, Germany) and hybridized to metaphase chromosomes. Hybridization signals for biotin-labeled probes were detected with avidin-fluorescein (Roche Diagnostics).

Real-Time Quantitative PCR

We quantified genomic DNA and mRNA using a real-time fluorescence detection method. Total RNA was obtained using Trizol (Invitrogen). Residual genomic DNA was removed by incubating the RNA samples with RNase-free DNase I (Takara Bio, Shiga, Japan) prior to reverse transcription (RT)-PCR. Single-stranded complementary DNA was generated using superscript III reverse transcriptase (Invitrogen) according to the manufacturer's directions. Real-time quantitative PCR experiments were performed with the LightCycler system using FastStart DNA Master Plus SYBR Green I (Roche Diagnostics) according to the manufacturer's protocol. The primers were as follows: *MAPK7* DNA (forward, 5′-TGCTGACTGGCTCGAAG-3′; reverse, 5′-GGGTCTGAGATGAACCTGC-3′); *MAPK7* mRNA (forward, 5′-TTTGCCTTACTTCCCACCTG-3′; reverse, 5′-CCCATGTCGAAAGACTGGTT-3′); *GRAP* mRNA (forward, 5′-TCGAAGGACAGACTGCACAC-3′; reverse, 5′-AGAAGAGGAGTGTGCCTCCA-3′); *EPN2* mRNA (forward, 5′-TCACCTCACCCACCACTGTA-3′; reverse, 5′-GTGGTCAGCTGCCCTTAGAG-3′); *EPPB9* mRNA (forward, 5′-CTTTGTGTACGGCCAGGACT-3′; reverse, 5′-CGTAGGGGTTGGTGCTTTTA-3′); *MFAP4* mRNA (forward, 5′-GGTGACTCCCTGTCCTACCA-3′; reverse, 5′-TCATCTCAGTGCGTTTGAGG-3′); *ZNF179* mRNA (forward, 5′-ACTGGGCAGAACCAGAGAGA-3′; reverse, 5′-AGGATGCACAGACAGGCTCT-3′); *FLJ10847* mRNA (forward, 5′-AACTCTTGGGCTTCAAGCAA-3′; reverse, 5′-AGGAGGTTGAGGCTGCAGTA -3′). These primers were designed using Primer3 (http://frodo.wi.mit.edu/cgi-bin/primer3/primer3_www.cgi) on the basis of sequence data obtained from the NCBI database (http://www.ncbi.nlm.nih.gov/). *GAPDH* (Minamiya et al., 2004) and long interspersed nuclear element (LINE)-1 (Zhao et al., 2004) were used as endogenous controls for mRNA and genomic DNA levels, respectively.

Immunoblotting

Immunoblots were prepared according to previously reported methods (Yasui et al., 2001). Cell lysates (20 μg protein per sample) were separated by sodium dodecyl sulfate-polyacrylamide gel electrophoresis on 10% acrylamide gels. We obtained the following antibodies from Sigma-Aldrich (Tokyo, Japan): anti-ERK5 polyclonal antibody, anti-phospho-ERK5 (pThr218/pThr220) polyclonal antibody, and anti-β-actin monoclonal antibody. For immunoblotting, we used anti-ERK5, anti-phospho-ERK5, and anti-β-actin at dilutions of 1:500, 1:1000, and 1:5000, respectively. For secondary immunodetection, we used anti-rabbit or anti-mouse Ig (Amersham, Tokyo, Japan) diluted 1:5000. Protein binding was detected using the ECL system (Amersham).

Immunoprecipitation

Cells were lysed with RIPA buffer (10 mM Tris-HCl, pH 7.4, 150 mM NaCl, 1% Triton X-100, 0.1% sodium dodecyl sulfate, 1% sodium deoxycholate, 1 mM phenylmethylsulfonyl fluoride), and incubated on ice for 30 min. The lysate was centrifuged at 14,000 × *g* at 4°C for 15 min. The supernatant was incubated with normal rabbit IgG and protein A-agarose beads (Santa Cruz Biotechnology, Santa Cruz, CA) to decrease nonspecific protein binding. After centrifugation, the supernatant was incubated with anti-ERK5 polyclonal antibody or normal rabbit IgG (control) overnight at 4°C. Protein A-agarose beads were added to the reaction and the mixture was incubated for an additional 1 hr. The precipitates were recovered by a brief centrifugation, followed by four washes with RIPA buffer. Samples were then boiled in electrophoresis sample buffer and separated by electrophoresis as described above (see "Immunoblotting" section).

Immunohistochemical Analysis

Forty-three primary HCCs, consisting of paired tumor and surrounding nontumor tissues, and two HCC cell lines (SNU449 and Li7) were analyzed by anti-ERK5 immunostaining. Immunohistochemical staining was performed on formalin-fixed and paraffin-embedded sections using an anti-ERK5 polyclonal antibody (Sigma-Aldrich) at a 1:200 dilution. An automated tissue immunostainer (Ventana Medical Systems, Tucson, AZ) was used according to the manufacturer's instructions. The staining was developed with 3,3′-

diaminobenzidine tetrahydrochloride, followed by counterstaining with hematoxylin.

Growth Assays and RNA Interference Studies

For cell growth assays viable cells were stained with 0.2% trypan blue and counted with a hemocytometer 24, 48, and 72 hr after transfection. For RNA interference (RNAi) studies, Stealth small interfering RNA (siRNA) duplex oligoribonucleotides targeting *MAPK7* (5′-CCAUGGCAUGAAC CCUGCCGAUAUU-3′) and Stealth RNAi negative control duplexes were synthesized by Invitrogen. The siRNAs were delivered into SNU449 cells using Lipofectamine 2000 (Invitrogen) according to the manufacturer's instructions. To determine mRNA levels, cells were harvested 48 hr after transfection and subjected to quantitative RT-PCR as described above.

Cell Cycle Synchronization

SNU449 cells were synchronized at G1/S, early S, or M phases. For G1/S or early S-phase synchronization, cells were incubated in medium containing 2.5 mM thymidine (Sigma Chemical Co., St. Louis, MO) for 24 hr, followed by 12 hr in medium without thymidine, and finally another 12 hr in medium containing 2.5 mM thymidine (double-thymidine block; for G1/S-phase) or 1 μg/ml aphidicolin (early S-phase block). For M phase synchronization, cells were incubated in medium containing 2.5 mM thymidine for 24 hr, followed by 4 hr in medium without thymidine, and finally another 12 hr in medium containing 0.5 μg/ml nocodazole.

Cell Cycle Analysis

SNU449 cells were synchronized at the G1/S-phase boundary by a double-thymidine block as described above. Synchronized cells were released into fresh medium without thymidine and harvested at the indicated time points. These cells were then stained with propidium iodide and analyzed using a FACSCaliber scanner and Cell Quest software (Becton Dickinson Pharmingen, San Diego, CA).

Mitotic Index

Cells were grown in 24-well plates and transfected with Stealth RNAi targeting *MAPK7* or Stealth RNAi negative control duplexes as described above (see "Growth Assays and RNA Interference Studies" section). After 24 hr, cells were synchronized at the G1/S-phase boundary by a double-thymidine block. Synchronized cells were collected, reseeded on glass slides, and incubated for an additional 9 hr in fresh medium without thymidine. Next, the cells were stained with an anti-phospho-histone H3 antibody that specifically detects mitotic cells. Briefly, cells were fixed with 3.7% formaldehyde, permeabilized with 0.25% Triton X-100, and incubated with PBS containing 1% bovine serum albumin. The cells were then treated with a mixture of 4 μg/ml anti-phospho-histone H3 (Ser10)-biotin conjugated antibody (Upstate Biotechnology, Lake Placid, NY) and a 1:100 dilution of streptavidin-fluorescein (Roche Diagnostics) for 1 hr at room temperature, followed by counterstaining with propidium iodide. Positive staining for phospho-histone H3 was quantified by counting stained cells under a fluorescence microscope and dividing by the number of total cells. The mitotic index was scored as the percentage of mitotic cells in a population. On average, 200 cells were scored in three separate areas.

Statistical Analysis

All statistical analyses were performed using SPSS 15.0 software (SPSS Inc., Chicago, IL). Chi-square tests or analysis of variance (ANOVA) were used. P values < 0.05 were considered significant.

RESULTS

Detection of the 17p11 Amplicon in HCC Cell Lines by SNP Array Analysis

We screened for DNA copy number aberrations in 20 HCC cell lines by SNP array analysis. Two of the 20 cell lines, SNU449 and JHH-7, exhibited amplifications at chromosomal band 17p11 (Fig. 1A). In particular, the SNU449 cell line showed a high level of amplification in a narrow region on 17p11. We were able to define the smallest commonly affected region in the 17p11 amplicon as that lying between the positions recognized by the Affymetrix SNP_A-1662618 and SNP_A-1720748 probes (Fig. 1B). This region includes seven known or predicted protein-coding genes, *GRAP*, *EPN2*, *EPPB9*, *MAPK7*, *MFAP4*, *ZNF179*, and *FLJ10847*. The size of the amplicon was estimated to be approximately 750 kb.

To confirm amplification at 17p11 in SNU449 cells, we performed FISH analysis. The probe for

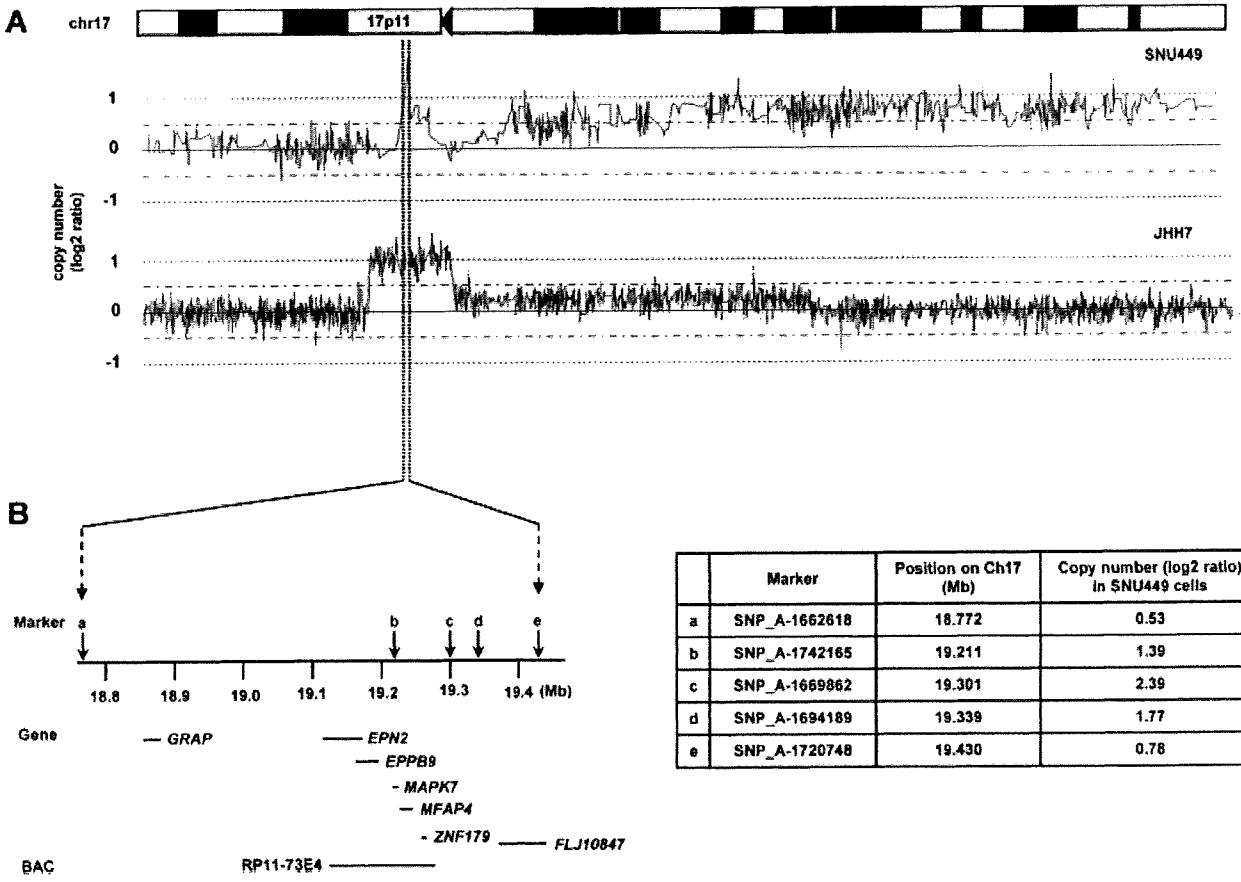

	Marker	Position on Ch17 (Mb)	Copy number (log2 ratio) in SNU449 cells
a	SNP_A-1662618	18.772	0.53
b	SNP_A-1742165	19.211	1.39
c	SNP_A-1669862	19.301	2.39
d	SNP_A-1694189	19.339	1.77
e	SNP_A-1720748	19.430	0.78

Figure 1. Map of the amplicon at 17p11 in two HCC cell lines. A: Copy number profiles for chromosome 17 in SNU449 and JHH-7 cells. Copy number values were determined by SNP 100K and 250K array analyses for SNU449 and JHH-7 cells, respectively. B: The smallest common region of amplification in SNU449 and JHH-7 cells (left). The position of the Affymetrix SNP markers, the seven genes within the amplicon (*GRAP*, *EPN2*, *EPPB9*, *MAPK7*, *MFAP4*, *ZNF179*, and *FLJ10847*) and the BAC RP11-73E4 (used as a probe for FISH) are numbered according to the UCSC genome database (http://genome.ucsc.edu/). Detailed copy-number information at positions identified by individual SNP markers over the amplified region in SNU449 cells is shown at right.

these experiments was BAC RP11-73E4, which contains *EPN2*, *EPPB9*, *MAPK7*, *MFAP4*, and *ZNF179* (Fig. 1B). This probe showed an amplified FISH signal on metaphase chromosomes from SNU449 cells (Fig. 2A). To further characterize the relationship between the genes in this chromosomal region and amplifications observed in cancer cells, we analyzed the gene dosage of the *MAPK7* locus by real-time quantitative PCR of DNA from 21 different liver cancer cell lines (20 HCC cell lines and the hepatoblastoma line HepG2). Amplification of *MAPK7* was observed in SNU449 and JHH-7 cells (Fig. 2B). Taken together, the data provide strong evidence that the 17p11 region is amplified in SNU449 and JHH-7 cells.

Analysis of Positional Candidate Genes in HCC Cell Lines

The 17p11 region may harbor one or more genes (henceforth referred to as "target genes") that, when activated by amplification, play a role in carcinogenesis. A common criterion for designating a gene as a putative target is that amplification leads to its overexpression (Collins et al., 1998). Thus, using real-time quantitative PCR, we determined the mRNA levels of all seven genes in the 17p11 amplicon in our panel of 21 liver cancer cell lines. As shown in Fig. 2C, the *EPN2*, *EPPB9*, and *MAPK7* genes were overexpressed in both SNU449 and JHH-7 cells. In several other lines, one or more of these three genes was overexpressed, despite the fact that regional amplification was not observed. These findings suggest that *EPN2*, *EPPB9*, and *MAPK7* are candidate target genes for 17p11 amplification.

Of these three genes, we chose to focus further analysis on *MAPK7*, which encodes ERK5, because ERK5-related proteins have been previously implicated in carcinogenesis (Hayashi and Lee, 2004; Wang and Tournier, 2006), whereas there is little or no evidence linking *EPN2* or

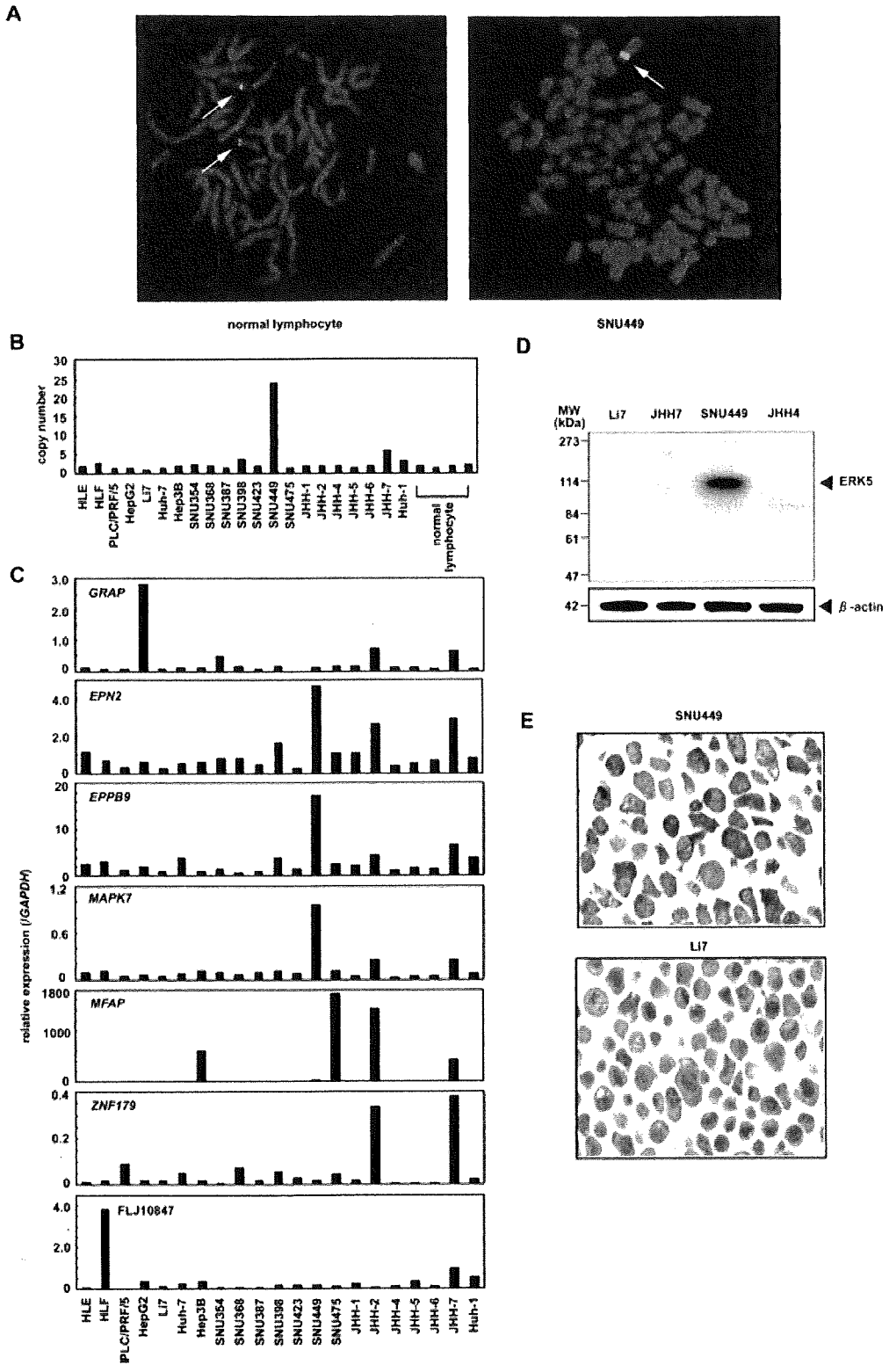

Figure 2. Amplification and overexpression of *MAPK7* in HCC cell lines. (A) Representative images from FISH analysis using a BAC RP11-73E4 probe on metaphase chromosomes from normal lymphocytes and SNU449 cells. While the probe shows a normal signal pattern (2 copies/cell) in normal lymphocytes (arrows, left), it shows an amplified signal in SNU449 cells (arrow, right). (B) Copy number of *MAPK7* in 21 liver cancer cell lines (20 HCC cells and one hepatoblastoma line, HepG2) and four peripheral blood lymphocytes (normal cell controls) as measured by real-time quantitative PCR with reference to a LINE-1 control. Values were normalized such that the average copy number of *MAPK7* in genomic DNA derived from normal lymphocytes is 2. (C) Relative expression levels of the seven genes within the 17p11 amplicon in a panel of 21 liver cancer cell lines as determined by real-time quantitative RT-PCR. The results are presented as the ratio between the expression level of each gene and a reference gene (*GAPDH*) to correct for variation in the amount of RNA. (D) Immunoblot analysis to detect protein levels of ERK5 and β-actin, an internal control, in four HCC cell lines with different *MAPK7* DNA copy numbers (B) and mRNA levels (C). (E) Immunostaining of ERK5 in SNU449 and Li7 cells.

EPPB9 to tumorigenesis. Immunoblot analysis revealed that ERK5 expression is upregulated in SNU449 cells. Indeed, among the HCC cell lines that were tested, SNU449 showed the highest level of both 17p11 amplification and *MAPK7* overexpression (Fig. 2D). Moreover, immunostaining confirmed that the level of ERK5 was elevated in SNU449 cells. ERK5 was strongly expressed in the cytoplasm of SNU449 cells (Fig. 2E). In contrast, ERK5 was weakly expressed in only a few Li7 cells, a HCC cell line that shows neither amplification nor overexpression of *MAPK7* (Fig. 2E).

Copy Number Gain of *MAPK7* in Primary HCC Tumors

To determine whether *MAPK7* is amplified in primary tumors, we examined 66 primary HCCs for copy number gains using real-time quantitative PCR. Copy number changes were counted as gains if the results of the analysis for a given tumor cell type exceeded the mean plus twice the standard deviation (SD) of the levels of *MAPK7* observed in genomic DNA derived from four peripheral blood lymphocyte samples (i.e., normal cells). A copy number gain for *MAPK7* was observed in 35 of the 66 tumors (53%; Fig. 3).

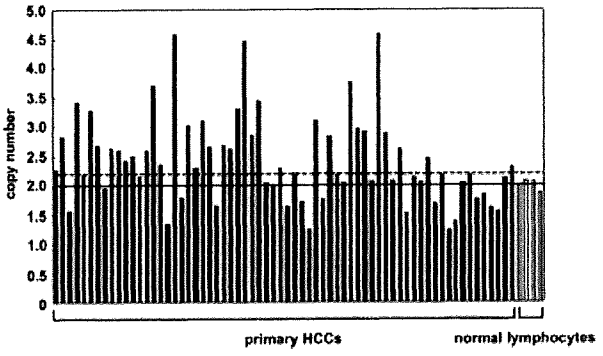

Figure 3. Copy number gain of *MAPK7* in primary HCC tumors. Copy numbers of *MAPK7* in 66 primary HCC tumors and four normal peripheral blood lymphocytes were determined by real-time quantitative PCR with reference to a LINE-1 control. Values were normalized such that the average copy number of *MAPK7* in genomic DNA derived from the normal lymphocytes equals 2 (solid horizontal line). The mean + 2 × SD of normal lymphocytes was used as the cutoff value for copy number gain (dotted line).

Expression of ERK5 in Primary HCCs

We next examined the level of ERK5 in 43 additional primary HCCs, including paired tumor and surrounding nontumor tissues. Immunohistochemical studies revealed that, in nontumor tissues (normal liver, chronic hepatitis, or liver cirrhosis), ERK5 is strongly expressed in bile ducts, bile ductules, and a few small hepatocytes (Fig. 4A). In these cells, ERK5 was present in the cytoplasm. Hepatocytes also contained ERK5, although at a lower level than in bile ducts (Fig. 4A). The staining pattern for ERK5 was almost identical for normal liver, chronic hepatitis, and liver cirrhosis.

This granular cytoplasmic staining for ERK5 was also observed in HCC cancer cells (Fig. 4B). HCC cells containing ERK5 were uniformly distributed in the tumor tissues. The level of ERK5 was elevated in 11 of the 43 tumors compared with the paired nontumor tissues (Figs. 4B and 4C; Supp. Info. Table 1). To clarify the relationship between the level of ERK5 and various clinicopathological parameters, we examined available data from the 43 patients, whose tumors were divided into elevated (T>NT) and not elevated (T≤NT) groups. There was no significant correlation between the level of ERK5 and any parameter examined, including age and gender of the patients; size, stage, and degree of differentiation of the tumor; HBV or HCV infection; and

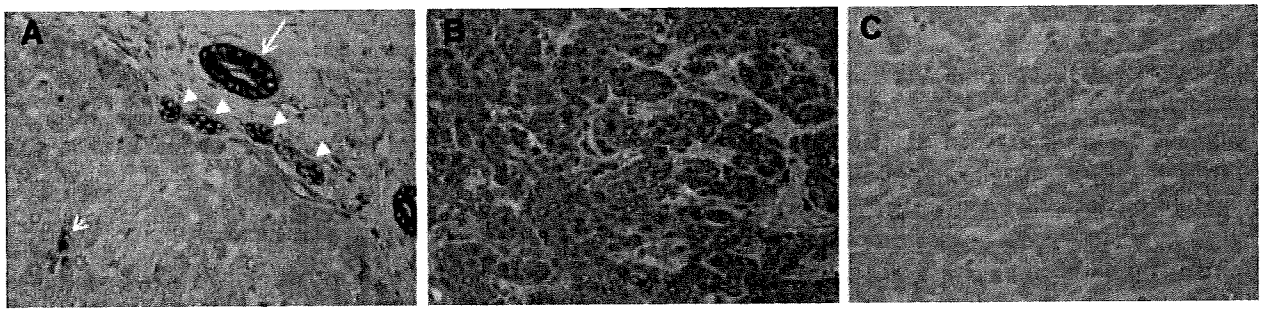

Figure 4. Representative ERK5 immunostaining of tissues. (A) A nontumorous liver tissue (chronic hepatitis). The level of ERK5 is elevated in the bile duct (large arrow), bile ductules (arrowheads), and a few small hepatocytes (small arrow). (B, C) Paired tumor (B) and nontumor (C) tissues from one HCC patient, wherein the level of ERK5 is elevated in the tumor compared with the counterpart nontumor tissue. Original magnification, ×400.